Renewable and Sustainable Energy Reviews 15 (2011) 24–46

Contents lists available at ScienceDirect

Renewable and Sustainable Energy Reviews

journal homepage: www.elsevier.com/locate/rser

Thermal conductivity enhancement of phase change materials for thermal energy storage: A review☆

Liwu Fan, J.M. Khodadadi *

Department of Mechanical Engineering, Auburn University, 270 Ross Hall, Auburn, AL 36849-5341, USA

ARTICLE INFO

Article history:
Received 30 June 2010
Accepted 2 August 2010

Keywords:
Fusible materials
Melting
Phase Change materials
PCM/Metal composites
Phase transformation
Solidification
Thermal conductivity enhancers

ABSTRACT

A review of experimental/computational studies to enhance the thermal conductivity of phase change materials (PCM) that were conducted over many decades is presented. Thermal management of electronics for aeronautics and space exploration appears to be the original intended application, with later extension to storage of thermal energy for solar thermal applications. The present review will focus on studies that concern with positioning of *fixed, stationary* high conductivity inserts/structures. Copper, aluminum, nickel, stainless steel and carbon fiber in various forms (fins, honeycomb, wool, brush, etc.) were generally utilized as the materials of the thermal conductivity promoters. The reviewed research studies covered a variety of PCM, operating conditions, heat exchange and thermal energy storage arrangements. The energy storage vessels included isolated thermal storage units (rectangular boxes, cylindrical and annular tubes and spheres) and containers that transferred heat to a moving fluid medium passing through it. A few studies have focused on the marked role of flow regimes that are formed due to the presence of thermally unstable fluid layers that in turn give rise to greater convective mixing and thus expedited melting of PCM. In general, it can be stated that due to utilization of fixed high conductivity inserts/structures, the conducting pathways linking the hot and cold ends must be minimized.

Contents

1. Introduction

Greater energy demand projected for developing economies, uncertainties associated with stable supply/pricing of fossil fuels and growing awareness of environmental issues have contributed to a serious re-examination of various renewable sources of energy. The unpredictability of the output of renewable energy systems demands that robust, reliable and efficient storage units must be an integral part of such energy systems. Among various forms of energy, thermal energy is widely encountered in nature as solar radiation, geothermal energy and thermally stratified layers in oceans. Thermal energy is also a by-product of a great number of

☆ *Disclaimer:* This report was prepared as an account of work partially sponsored by an agency of the United States Government. Neither the United States Government nor any agency thereof, nor any of their employees, makes any warranty, express or implied, or assumes any legal liability or responsibility for the accuracy, completeness, or usefulness of any information, apparatus, product, or process disclosed, or represents that its use would not infringe privately owned rights. References herein to any specific commercial product, process, or service by trade name, trademark, manufacturer, or otherwise does not necessarily constitute or imply its endorsement, recommendation, or favoring by the United States Government or any agency thereof. The views and opinions of authors expressed herein do not necessarily state or reflect those of the United States Government or any agency thereof.

* Corresponding author. Tel.: +1 334 844 3333; fax: +1 334 844 3307.
E-mail address: khodajm@auburn.edu (J.M. Khodadadi).

1364-0321/$ – see front matter © 2010 Elsevier Ltd. All rights reserved.
doi:10.1016/j.rser.2010.08.007

Table 1
Summary of studies on thermal conductivity enhancement of PCM/enhancer composites.

Authors (year)	PCM		Promoter			Configuration		Study/Measurement Technique
	Material	Properties	Material	Size	Properties	Vol.%[a]	Type	
Bentilla et al. [11] (1966)	1. tetradecane	MT[b]: 278.8	1. Al wool	N/A	N/A	10–18	N/A	experiments
	2. hexadecane	MT: 289.9	2. Al foam	N/A	ρ: 900	N/A	N/A	
	3. octadecane	MT: 301.0	3. Cu foam	N/A	ρ: 500	N/A	N/A	
	4. eicosane	MT: 309.9	4. Al honeycomb	N/A	N/A	N/A	N/A	
Hoover [12] (1971)	$LiNO_3$–$3H_2O$	MT: 300	1. Al powder	N/A	N/A	12.5 (no volume or mass-based information)	N/A	DSC measurements
		LH[c]: 232.4 k: 0.519 c_p: 1.6736 ρ: 1,602	2. Al gauze 3. Al honeycomb 4. alumina (Al_2O_3) foam 5. alumina powder					
Humphries [13] (1974)	nonadecane	MT: 305.3	Al fins	details in paper	N/A	N/A	vertically mounted	1. thermocouples
Griggs et al. [14] (1974)	nonadecane	N/A	Al	N/A	N/A	N/A	N/A	2. visual observation transient 2D numerical study (diffusion only)
Abhat [15] (1976)	octadecane ($C_{18}H_{38}$)	MT: 301.5	Al honeycomb	details in paper	N/A	≈ 11.5% (estimated by us)	N/A	1. Iron-Constantan thermocouples 2. transient non-equilibrium numerical study (diffusion only)
De Jong and Hoogendoorn [16] (1981)	1. pure paraffin (n-eicosane $C_{20}H_{42}$)	MT: 310	1. Al honeycomb	N/A	N/A	10%	N/A	1.caloric method
		LH: 125 k: 0.2 (L) and ≈ 0.10 (S) c_p: 2.3 (L[d]) and 2.4 (S)						2. dynamic DTA 3. THW[e] 4. transient cylinder 5. thermocouples 6. enthalpy method
	2. commercial wax	MT: 315 ∼ 317	2. Al thin-strip matrix	compacted as required	N/A	0.4, 0.8, and 1.6%	N/A	
		LH: ≈ 137 k: 0.19 (L) and ≈ 0.14 (S) c_p: 2.4 (L) and 2.2 (S)						
Abhat et al. [17] (1981)	1. eicosane	MT: 310	Al metal fins	N/A	N/A	N/A	longitudinally positioned	1. NiCr-Ni thermocouples 2. visual observation
	2. lauric acid	MT: 315 ∼ 317						
	3. $CaCl_2{\cdot}6H_20$	MT: ≈ 303						
Henze and Humphrey [18] (1981)	octadecane ($C_{18}H_{38}$)	MT: 301	Al fins	flat plate (thickness = 0.0625, 0.09375, and 0.125 inches)	k: 179.962	N/A	symmetrically positioned	1. 2D transient model
		LH: 241.36			c_p: 0.96			2. iron-constantan thermocouples
		k: 0.149 (L) c_p: 2.66 (L) ρ: 777 (L) and 852.8 (S) β[f]: 0.001			ρ: 2,712.6			3. visual observation

Table 1 (*Continued*)

Authors (year)	PCM		Promoter			Configuration		Study/Measurement Technique
	Material	Properties	Material	Size	Properties	Vol.%[a]	Type	
Haji-Sheikh et al. [20,21] (1983, 1984)	commercial wax (SUNTECH P116), a mixture of C_{20} through C_{32} hydrocarbons	MT: 317 LH: 226 ∼ 266 k: 0.193 ∼ 0.24 (L) and 0.24 (S) c_p: 2.51 (L) and 2.95 (S) ρ: 748 ∼ 790 (L) and 818 (S) β: 0.00204 ∼ 0.00216	N/A	flat plate	N/A	N/A	evenly positioned	1. thermocouples 2. flow visualization
Knowles and Webb [22] (1987)	1. hexadecane	k: 0.15 c_p: 2.42 ρ: 760	Al	plate fins or wires	k: 240 c_p: 0.926 ρ: 2,700	1, 26, and 50%	uniformly distributed	1. transient lumped model 2. platinum resistance thermometer
	2. dodecanol	MT: 295.8 volumetric LH: 171 [MJ/m^3]	Cu	N/A	N/A	0, 1.4, 8.9, 50%	uniformly distributed	
Chow et al. [23] (1996)	LiH	MT: 958 LH: 2,580 k: 2.1 (L) and 4.2 (S) c_p: 7.37 (L) and 6.28 (S) ρ: 550 (L) and 690 (S)	Ni (S)	N/A	k: 92.1 c_p: 0.439 ρ: 8,913	5%	uniformly mixed	steady-state numerical study (diffusion only)
Tong et al. [24] (1996)	water/ice	k: 0.575 (L) and 2.21 (S) c_p: 4.217 (L) and 2.04 (S) ρ: 999.9 (L) and 917 (S)	Al matrix	N/A	k: 237 c_p: 0.896 ρ: 2,707	5, 10, and 15%	uniformly distributed, water/ice fully saturated	transient numerical study (diffusion and convection)
Bugaje [25] (1997)	paraffin wax	MT: 331 ∼ 333 LH: 266 k: 0.24 (L) and 0.24 (S) c_p: 2.51 (L) and 2.95 (S) ρ: 760 (L) and 818 (S)	Al matrix	N/A	N/A	6% and 20%	N/A	thermocouples
Pal and Joshi [26] (1998)	*n*-triacontane	MT: 338.6 LH: 251 k: 0.23 c_p: 2.05 ρ: 810	Al honeycomb	side length: 1.65 mm height: 14.5 mm	N/A	N/A	fully filled	1. T-type thermocouples 2. numerical study (conjugate, diffusion and convection)
Velraj et al. [28] (1999)	paraffins RT 58 and 60	LH: 214.4 k: 0.2 c_p: 0.9 ρ: 775 (L) and 850 (S)	1. Al fins	N/A	N/A	7% and 20%	internal longitudinal cross shaped cross-section	1. K-type NiCr-Ni thermocouples 2. parameter estimation 3. numerical study (enthalpy method)
			2. lessing rings	d: 1 cm			randomly distributed	
			3. water bubbles	N/A				

Fukai et al. [29,30] (1999, 2000)	paraffin wax	MT: 314 ∼ 316 k: 0.26 (S)	carbon fibers	l: 5, 200 mm d: 10 μm	k: 220 ρ: 2,170	< 2%	1. randomly positioned 2. fiber brush in radial direction	1. thermocouples 2. parameter estimation
Cabeza et al. [31] (2002)	deionized water	LH: 330 k: ≈ 0.6 (L) and ≈ 2.4 (S) c_p: ≈ 4.1 (L) ρ: ≈ 1000 (L)	1. stainless steel	tube pieces l: 25 mm d: 16 mm (inner), 18 mm (outer)	k: 45 c_p: 0.4 ∼ 0.5 ρ: 7,800	< 10%	N/A	thermocouples
			2. Cu		k: 393 c_p: 0.383 ρ: 8,900			
			3. graphite matrix	N/A	k: 25 ∼ 470 c_p: 1.4 ρ: 2,300			
Ettouney et al. [32] (2004)	paraffin wax	MT: 325 LH: 210 k: ≈ 0.15 (L) and ≈ 0.24 (S) c_p: ≈ 2.1 (L) and ≈ 2.9 (S) ρ: ≈ 860 (S) and ≈ 780 (S)	1. stainless steel screens	l: 0.32 m w: 0.02 m	k: 40 c_p: 0.5 ρ: 7,801	0.1% ∼ 3.4%	radially positioned (60°, 180°, and 300°)	thermocouples
			2. stainless steel spheres	d: 8, 12, and 16 mm			attached to metal screens	
Stritih [33] (2004)	paraffin RT 30	MT: ≈ 306	steel fins	0.5 m (h) × 0.12 m (l) × 1 mm (thickness)	k: 20	≈ 5%	fins evenly spaced	NiCr-Ni thermocouples
Koizumi [34] (2004)	n-octadecane	MT: 301 LH: 244 k: 0.15 (L) and 0.21 (S) ρ: 733 (L) and 890 (S)	Cu plates	N/A	N/A	N/A	cross-shaped fins	Cu-Co thermocouples Flow visualization
Mesalhy et al. [35] (2005)	generic PCM	MT: 300.4 $k(S)/k(L) = 2.419$ $c_p(S)/c_p(L) = 0.964$ $Pr = 46.1$	high conductivity solid matrix	N/A	k(matrix)/k(PCM) = 50, 100, and 200	5, 10, and 15%	rectangular cells with conductive fibers making up the sides	thermal non-equilibrium numerical study
Ettouney et al. [37] (2006)	paraffin wax	MT: 325 LH: 210 k: 0.15 (L) and 0.24 (S) c_p: 2.1 (L) and 2.9 (S) ρ: 780 (L) and 860 (S)	stainless steel spheres	d: 4, 5, and 6 mm	k: 20 c_p: 0.46 ρ: 7,846	N/A	accumulated on the bottom	K-type thermocouples
Nayak et al. [38] (2006)	eicosane	MT: 310 LH: 241 k: 0.157 (L) and 0.39 (S) c_p: 2.2 (L) and 1.9 (S) ρ: 770 (L) and 810 (S)	1. Al matrix	$d = 420$ μm	k: 179.6 c_p: 0.96 ρ: 2,712.9	5, 10, and 15%	uniformly filled with PCM	transient numerical study (diffusion and convection)
			2. Al fins	see Fig. 30		10, 20, and 30%	1. plate-type (2-D) 2. rod-type evenly spaced (3-D)	

Table 1 (*Continued*)

Authors (year)	PCM		Promoter		Configuration			Study/Measurement Technique
	Material	Properties	Material	Size	Properties	Vol.%[a]	Type	
Nakaso et al. [39] (2008)	paraffin wax	MT: 322.2 LH: N/A k: 0.12 (L) and 0.21 (S) c_p: N/A ρ: 780 (L) and 900 (S)	Woven carbon fiber sheets and carbon fiber brushes	10 μm in diameter fibers	k: 190 c_p: 1 ρ: 2,120	0.21 & 0.42 for sheets/0.75 for brushes	1. cloth wrapping copper tubes 2. radially-pointing fiber brushes	1. inlet/outlet temperature measurements 2. transient modeling of conduction
Agyenim et al. [40] (2009)	erythritol ($C_4H_{10}O_4$)	MT: 390.9 LH: 339.8 k: 0.326 (L) and 0.733 (S) c_p: 2.76 (L) and 1.38 (S) ρ: 1300 (L) and 1480 (S)	Cu plates used as circular and longitudinal fins	1 mm (thickness)	N/A	Not given but can be computed	radial and longitudinal fins	1. DSC measurements 2. K-type thermocouples

[a] Vol.% denotes the volume fraction (%).
[b] MT denotes the melting temperature (K).
[c] LH stands for the latent heat (kJ/kg), k is thermal conductivity (W/mK), and ρ is density (kg/m^3).
[d] L stands for the liquid phase and S for the solid phase, unit for specific heat c_p is kJ/kg K.
[e] THW denotes the transient hot-wire method.
[f] Thermal expansion coefficient (1/K).

man-made energy conversion systems, equipment and devices. Despite its abundance, thermal energy is generally classified as a low-grade form of energy and is associated with waste in industrial processes. Storage of thermal energy may simply serve as a holding station before it is used properly or it can be a means of providing thermal comfort in buildings, conserving of energy in various sectors of the economy, increasing the operational life of electronics and raising the efficiency of industrial processes.

1.1. Phase change materials for thermal energy storage

Thermal energy can be stored as sensible or latent energy by heating or cooling a bulk of material. This energy then becomes available when the reverse process is applied. Phase change materials (PCM) are widely used to store thermal energy at a fixed temperature by taking advantage of their latent heat (heat of fusion) during phase change. The melting temperature varies over a wide range for different PCM, e.g., paraffins, fatty acids, sugar alcohols, salt hydrates, etc. A number of review articles [1–9] discussed candidate PCM, their thermophysical/transport properties, encapsulation, heat transfer enhancement and system-related issues. The coverage of heat transport mechanisms encountered in phase change systems that are discussed in these reviews is deemed to be narrow (except ref. [9]), at times only limited to listing of some references. In view of this observed shortcoming and based on the greater importance of thermal energy storage and associated developments in related fields, the present review of literature with a focus on thermal conductivity promotion of PCM was prepared.

2. Options for promotion of thermal conductivity of PCM

An undesirable property of PCM is their relatively low thermal conductivity that strongly suppresses the energy charging/discharging rates. Naturally, introduction of highly conductive materials to form a composite of the PCM and thermal conductivity promoter is a logical solution. The insertion of metal fins, foams, wools into the PCM has long been practiced. Determining proper configurations of these *fixed, non-moving* structures and their interactions with conduction, convection and phase change heat transport mechanisms pose challenging issues. Literature devoted to thermal conductivity enhancement through utilization of non-moving structures goes back many decades. The bulk of this manuscript is devoted to providing a review of major findings in relation to competing heat transfer mechanisms in such systems.

3. Scope and coverage of the present review

The primary focus of the present review will be on the thermal conductivity enhancement that is realized through introduction of *fixed, non-moving* high-conductivity inserts. Therefore, no coverage of *free-form, fluid-like, evolving* composites (e.g. particle-dispersed systems) will be provided. Metal foam and graphite-based PCM systems are getting a great deal of attention, however only a few papers on such thermal conductivity enhancement approaches will be covered in this review. The exposition of reviewed work on thermal conductivity enhancement of PCM will be presented in a chronological order. This is reasoned to be appropriate since it is assumed that researchers generally get acquainted with prior work and their attributes/shortcomings before moving forward. An elaborate Table 1 that summarizes the relevant details for the reviewed papers are provided. A summary of the configurations of the experimental setups and the thermal operating conditions is given in Table 2. All the figures (except Figs. 1–4, 13 and 14) and artwork in this manuscript are taken from the reviewed papers and the authors do not take responsibility for their quality. At times,

Table 2
Summary of experimental configurations and thermal operating conditions of reviewed studies in the literature.

Paper	Geometry	Insulated Surfaces	Volume[a]	Phase Change	Heating/Cooling Scheme	Thermal Conditions	Gravity/HF angle[b]
Abhat [15]	Rectangular box	5[c]	2,166	Melting	***H***:[d] CHF[e] MINCO heater foil	0.03 to 0.325 W/cm^2	180°
De Jong and Hoogendoorn [16]	Cylindrical tube	T B[f]	347	Freezing	***T***: outer water stream	10 to 20 °C below melting temp.	90°
	Annular tube	S	377		***T***: inner tube heat exchanger	somewhat below melting temp.	90°
Abhat et al. [17]	Annular tube	T B	750	Melting	***T***: CT at one end of heat pipe	kept at 50 °C	0° ∼ 180°
				Freezing	***T*** : CT outer liquid flow	kept at 15 °C	
Henze and Humphrey [18]	Rectangular box	3	103	Melting	***T*** : CT MINCO heater foil	kept at 5, 10, 15 and 20 °C above melting temp.	90°
Eftekhar et al. [20]	Rectangular box	4	55.4	Melting	***T*** : CT hot and cold plates	kept the top (cold) and bottom (hot) walls at various temp. gradients	180°
Knowles and Webb [22]	Cylindrical tube	T S	393	Melting	***H***: CHF copper heater plate	kept at 12.7 kW/m^2	180°
Bugaje [25]	Cylindrical tube	T B	270	Melting	***T***: outer air flow	69 to 81 °C	90°
				Freezing		25 to 45 °C	90°
Pal and Joshi [26]	Rectangular box	5	292.4	Melting	***H*** : CHF silicone rubber patch heater	increased from 15 to 60 W at a step of 5 W	180°
Velraj et al. [28]	Cylindrical tube	N/A	1,374	Freezing	***T*** : CT water bath	kept at 50, 54 and 55 °C	90°
Fukai, et al. [29,30]	Cylindrical tube	T B	255	Melting	***T*** : CT water bath	20 to 60 °C	90°
				Freezing			
Cabeza et al. [31]	Rectangular box	5	4,647	Melting	***T*** : CT planar heat exchanger	kept at 15 °C	90°
				Freezing		kept at–15 °C	90°
Ettouney et al. [32]	Annular tube	S	1,534	Melting	***T*** : inner tube heat exchanger	70, 80 and 90 °C inlet temp. 0.171 kg/s mass flow rate	90°
Stritih [33]	Rectangular box	5	39,000	Melting	***T*** : planar heat exchanger	65 °C inlet temp.	90°
				Freezing		18 °C inlet temp.	90°
Koizumi [34]	Spherical container	N/A	58	Melting	***T*** : outer air flow	20 °C above melting temp.	180°
Ettouney et al. [37]	Spherical container	N/A	11.5	Melting	***T*** : outer air flow	70, 80 and 90 °C inlet temp.	180°
Agyenim et al. [40]	Annular tube	N/A	14,500	Melting	***T*** : heat exchange with silicone oil	140 °C inlet temp.	90°
				Freezing	***T*** : heat exchange with water	70 °C inlet temp.	

[a] This column gives the total volume occupied by both PCM and promoters [unit: cc].
[b] This column provides the angle between the gravitational acceleration vector and heat fluxes (HF).
[c] The number in this column specifies how many surfaces are insulated when a rectangular box is being investigated.
[d] ***H*** means the heat flux input is known and ***T*** means the surface temperature is known.
[e] CHF denotes constant heat flux and CT denotes constant temperature.
[f] T, B and S stand for the top, bottom and side walls of a cylindrical or annular tube, respectively.

some items such as arrows are added to the artwork in order to clarify the original figures and/or highlight the point that is being emphasized by the present authors.

4. Thermal conductivity enhancement through introduction of stationary structures

The literature reviewed in this broad category covers a variety of approaches. A chronological review of literature is adopted in order to allow the reader to appreciate the advancement of the prevailing technology and/or its emergence in response to new applications.

4.1. Early work inspired by heat rejection issues in space exploration systems

Early work on thermal control and energy storage using PCM can directly be linked to the fast-paced developments in aeronautics and electronics in the middle of the twentieth century that was followed by the Space Program. A NASA document authored by Humphries and Griggs [10] provided a good overview of the state-of-the-art at that time and is widely referenced in a number of papers on thermal storage and PCM. Relevant to the focus of this review article on thermal conductivity promoters, Humphries and Griggs [10] discussed a number of earlier work on utilization of metallic "fillers" to enhance the thermal conductivity of PCM. Bentilla et al. [11] outlined attempts to use filler materials such as metallic wool, foam and honeycomb. Tetradecane, hexadecane, octadecane and eicosane were the four fusible materials that were utilized along with compressed aluminum wool (10 and 18% bulk volume), aluminum foam (density of 900 kg/m^3), copper foam (density of 500 kg/m^3) and aluminum honeycomb. The honeycomb option provided a more effective heat transfer fin that may be chosen in various thicknesses due to its versatility in its extreme expanded and unexpanded conditions.

Hoover et al. [12] reported results of experimental studies pertinent to spacecraft thermal control with a number of pure PCM and PCM/composites with metals and other materials. The experiments focused on PCM system performance characteristics, determination of PCM and PCM/filler thermal diffusivities, the effects of long-term thermal cycling, PCM-container compatibility, catalyst effectiveness and stability. Three PCM were found acceptable to be considered for use in prototype aluminum thermal control devices. These three PCM were lithium nitrate trihydrate ($LiNO_3$–$3H_2O$) with zinc hydroxy nitrate catalyst, acetamide and myristic acid. Using $LiNO_3$–$3H_2O$ as the PCM, aluminum powder, aluminum gauze, aluminum honeycomb, alumina (Al_2O_3) foam and alumina powder were used as fillers with 8/1 PCM/filler ratio. No details of this ratio being volume or mass-based were provided. Moreover, no details on size of the powders were given. Among the fillers tested, aluminum honeycomb exhibited the greatest increase in system thermal diffusivity of about 80%. A procedure was proposed to assess the effects of thermal cycling (50 melting/freezing cycles) on properties of the PCM evaluated using repetitive (differential scanning calorimetry (DSC) measurements. Moreover, the effects of thermal cycling on the test containers were examined. In a series of tests using DSC, effects of the heating rates (1.2, 2.5, 5, 10 and 20 °C/min) were examined consecutively to melt Oxazoline Wax TS970 for a total of 10 melting cycles. For all the tests, the melting points were unchanged and no signs of degradation were noticed.

Humphries [13] designed a transparent test specimen that allowed for visual observation of the phase change interface. The housing that contained the nonadecane paraffin also included aluminum fins that partitioned the compartment into cells. Thermocouple readings within the paraffin, on the fins and other positions were compared to computational models of the phase change that combined a diffusive model in combination experimental correlations for natural convection.

Griggs et al. [14] reported results of their numerical investigation of conductive heat transfer of the melting process inside a rectangular container filled with PCM. Parallel plate fins of uniform thickness were placed inside the container in order to enhance the internal heat transfer rate. Because of the periodical design feature, the computational domain was limited to a single cell. The energy equation was non-dimensionalized and a group of dimensionless ratios were introduced to obtain a generic numerical model for this two-dimensional pure-conduction phase change problem. Very detailed numerical formulations and procedures were given in this paper. A parametric study was conducted for a special case that aluminum and nonadecane were used as base plate/fin material and PCM, respectively. With no subcooling, the heat flux load on the base aluminum plate was varied, whereas the opposite plate was insulated. At the terminal instant of melting, the ratio of total stored heat energy to latent heat energy as a function of the fin geometric ratio, which is defined as half cell width divided by fin width, was presented. The results suggest that the heat transfer rate is enhanced as the fin width increases and the contribution of latent energy to the total storage decreases. The temperature rise of the base above the melting temperature at the termination of melting was also investigated and a range of optimum fin geometric ratio that promised minimum temperature rise was suggested.

A PCM-based thermal capacitor with a honeycomb filler was designed and investigated by Abhat [15]. Aluminum and *n*-octadecane ($C_{18}H_{38}$) were employed as the container/honeycomb filler material and PCM, respectively and the experimental setup was described in detail. A side-view of the structural configuration of the capacitor with net dimensions of 288 mm × 188 mm × 40 mm is shown in Fig. 1, which was filled with parallel honeycombs of uniform size. The nominal heat storage capacity of this device was about 100 Watt-hours. In order to avoid undesirable contact thermal

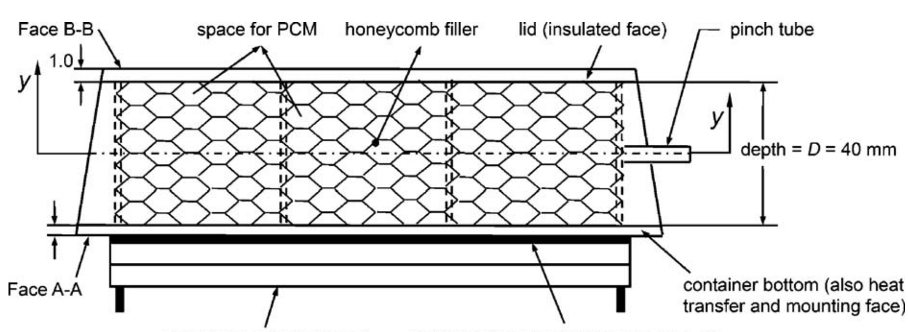


Fig. 1. Schematic diagram of the experimental setup of the honeycomb-packed PCM capacitor (reproduced from Abhat [15]).

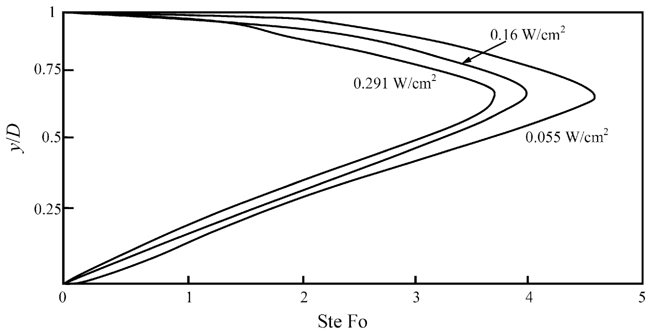


Fig. 2. Predicted position of the melting fronts as a function of dimensionless time for different heat inputs (Abhat [15]).

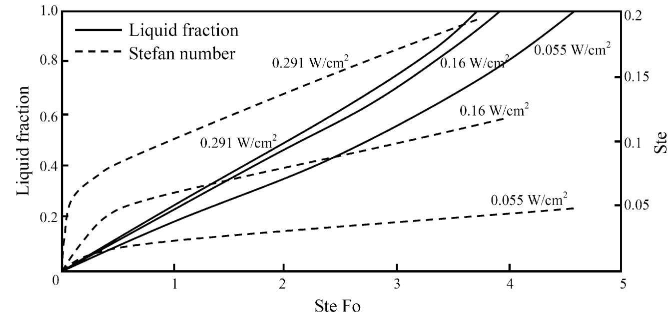


Fig. 3. Predicted molten fraction as a function of dimensionless time for different heat inputs (Abhat [15]).

resistance, honeycombs and container walls were bonded using an epoxy (Eccobond) with high thermal conductivity. Gas-free liquid PCM was filled into the evacuated container through pinch tubes that were connected to one of the side walls. Ten iron-constantan thermocouples were mounted at different locations both on the top and bottom surfaces. A MINCO foil resistance heater that had the same size as the bottom surface and served as the plane constant heat flux source was attached on that surface and the remaining five walls were insulated. Ignoring convection effects, a finite-difference-based lumped capacity thermal non-equilibrium numerical model was developed to predict the two-dimensional phase change heat conduction inside the container. Applying both experimental and numerical approaches, time-dependent variations of wall temperatures, interface location and molten fraction were studied. As shown in Fig. 2, predictions suggest that melting initiates on both the heated bottom and the insulated top surfaces due to the presence of aluminum honeycombs that serve as a heat path between the two surfaces. This is also beneficial since it gives rise to lower temperature non-uniformity within the device. The variation of molten fraction with the product of the Stefan and Fourier numbers, which is a dimensionless time variable, for three different input heat fluxes is sketched in Fig. 3. As the heat flux is increased, the melting rate accelerates. Additionally, the predicted maximum temperature on both the bottom and top surfaces at the instant of complete melting as a function of heat input are plotted in Fig. 4, in which deviations between the experimental and numerical results are apparently observed possibly due to the heat convection effect in each honeycomb cell that was neglected in the numerical approach.

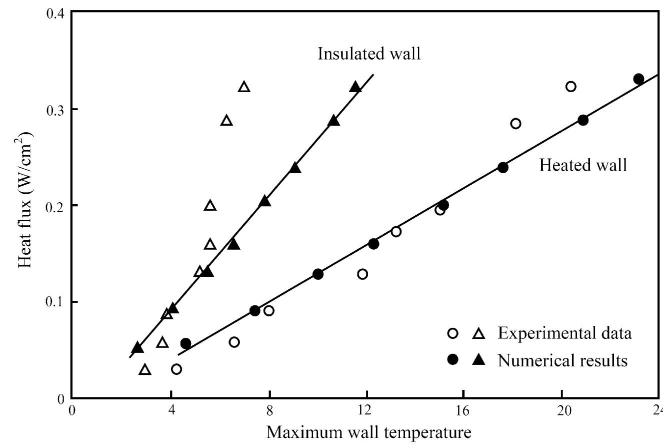


Fig. 4. Maximum temperature on both bottom and top surfaces at the instant of complete melting as a function of heat input (Abhat [15]).

4.2. Extension to solar thermal and thermal management of electronics applications

De Jong and Hoogendoorn [16] utilized two kinds of metal materials and two enhancement approaches to improve the heat

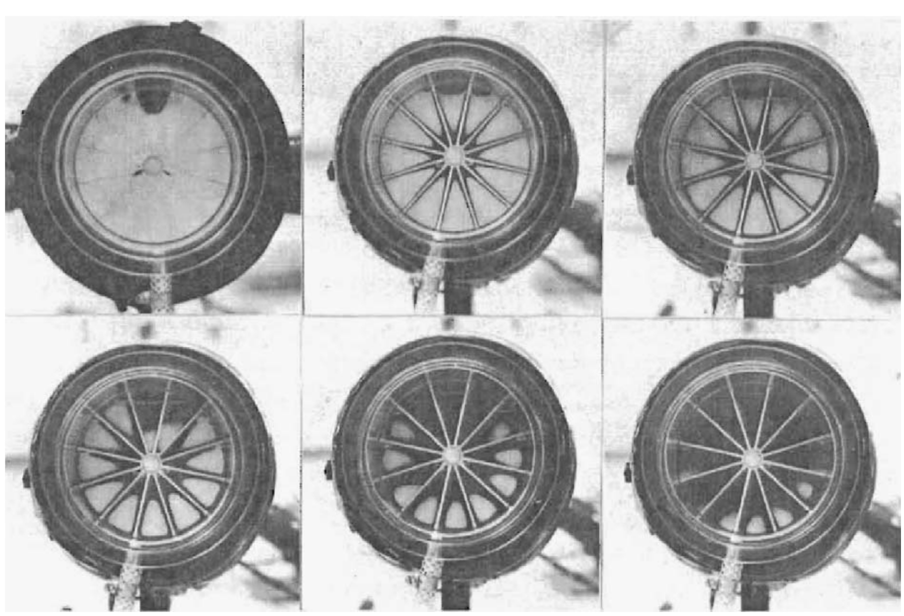


Fig. 5. A sequence of photos depicting the transient melting process of the test model with eicosane (Abhat et al. [17]).

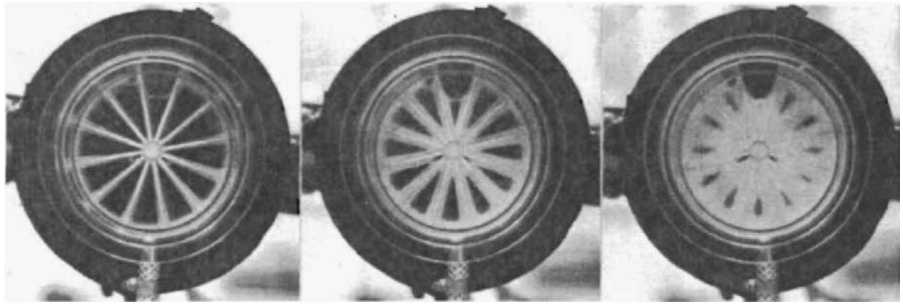


Fig. 6. A sequence of photos showing the transient solidification process of the test model with eicosane (Abhat et al. [17]).

transport of latent heat storage systems, as well as several methods to measure or estimate the enhancement effectiveness. The PCM involved in this study were pure eicosane ($C_{20}H_{42}$) and a commercial wax. First, they employed the caloric method and dynamic differential thermal analysis (DTA) method to measure the heat capacities of PCM. In the measurements, the secondary latent heat effects have been investigated for both materials. Then, they measured the thermal conductivity of PCM by using two different approaches, which are the transient hot-wire method for both liquid and solid phases and the transient cooling/heating cylinder method for the solid phase, respectively. The first enhancement technique was the application of finned copper tubes, which resulted in a very good effect on the decrease of solidification times of the systems because the heat exchange area was greatly increased. The second technique was to add metal matrix structures to PCM systems. The aluminum honeycombs (volume fraction of 10%) and aluminum thin-strip matrices (volume fraction of 0.4, 0.8 and 1.6%) were both utilized. Based on the experimental results, both structures can apparently reduce the solidification times with a factor up to 7. Compared to the original PCM, the thermal conductivity of the enhanced PCM was also apparently increased. Finally, they proposed a computational enthalpy method to estimate the heat transfer during the solidification process. The numerical results were able to give good agreement to the measured data. This paper was mainly focused on the experimental study, however, some details about the experimental configurations were not discussed, e.g. the procedure of preparing and adding the enhanced metal matrices.

Abhat et al. [17] presented an experimental study of a heat-of-fusion storage system for solar heating applications (290–350 K temperature range). The first half of this paper discussed heat storage materials. Melting temperature, energy absorption rate and energy evolution rate, for some typical materials were investigated using DSC. A more detailed study of the characteristics and choices of heat storage materials can be found in Abhat [1]. In this experiment, eicosane, lauric acid and $CaCl_2{\cdot}6H_2O$ were selected as storage materials. A finned-annulus heat exchanger, in which aluminum metal fins were positioned radially, was used as the container filled with PCM. A small test model with a length of 0.1 m that was proportionally similar to a practical system was built. Thirty NiCr–Ni thermocouples were mounted to measure the temperature distribution inside the test model. However, the positions of these thermocouples were not mentioned. Both the transient melting and freezing processes were visually investigated through the transparent covers made of Plexiglas flanges. During the melting process with eicosane, photos of the visualized interface variation inside the test model were taken (shown in Fig. 5). Although the existence of fins suppressed natural convection, it is shown clearly that heat convection still occurred, especially in the upper part of the sector. In comparison, the pictures showing the interface variation during the solidification process were also taken. As shown in Fig. 6, in contrast to the apparently asymmetric interface fronts during melting, symmetric frozen interface fronts in each segment were observed during the entire solidification process suggesting dominance of heat diffusion. The test model was heated via a heat pipe mounted in the inner tube, whereas solidification was driven by cool water around the outer surface. The temperature potential, which was the difference between the hot water temperature and the melting temperature, versus the maximum temperature difference inside the chamber and charging time was sketched in Fig. 7. As the temperature potential was increased, the charging rate accelerated and the maximum temperature difference decreased, which indicates that heat convection effects were enhanced. The paper also reported on the potential and economics of the practical application of this storage system.

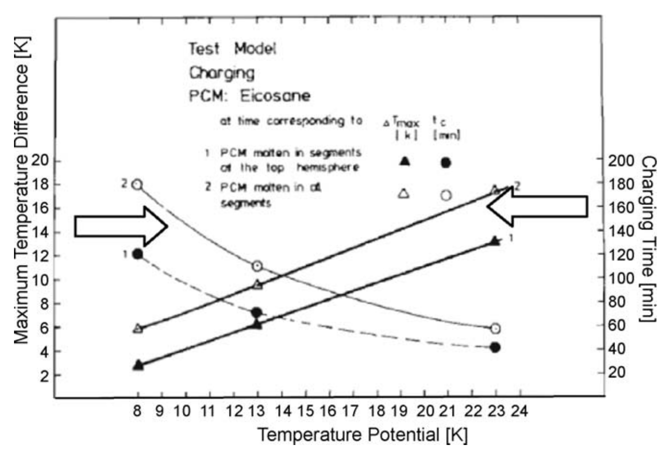


Fig. 7. Temperature potential versus maximum temperature difference and charging time for the test model with eicosane (Abhat et al. [17]).

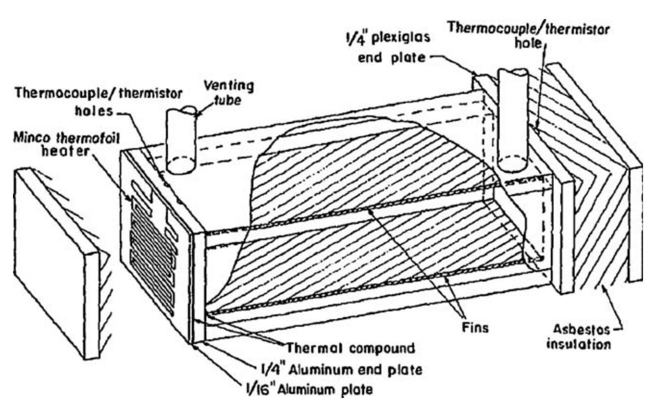


Fig. 8. Schematic diagram of the experimental test section (Henze and Humphrey [18]).

Henze and Humphrey [18] proposed a simple two-dimensional heat conduction model for predicting the melting rate and melting interface location of finned PCM storage devices. In order to validate this model, the authors designed and conducted visualized melting experiments of a double-finned rectangular Plexiglas container of inside dimensions 12.70 cm × 2.54 cm × 3.18 cm, which was filled with octadecane. As shown in Fig. 8, one end of the container was insulated, whereas the thermally active end was well-bonded to a MINCO foil heater. It should be noted that the entire test section was placed in a constant-temperature air bath that remained at a temperature 1 °C below the melting point of octadecane. This arrangement was used to minimize the heat loss from the container to the environment and realize negligible heat conduction in the solid phase. An electronic circuit was designed to control the heater, thus maintaining a constant temperature on the active end. Eight 24-gauge iron-constantan thermocouples were used to monitor the end conditions and the thermal status of the air bath. During the freezing process, the PCM was degasified by vibrating the test section on a high-frequency shaker table. Eleven runs were conducted for different combinations of the active wall temperature and fin thickness. A typical time progression of the melting liquid–solid interface for the case without fins was shown in a sequence of photographs (Fig. 9). The asymmetric interface is clearly indicative of the presence of convective currents that would not have been present for the case of pure conduction. The white arrows that are drawn by the present authors in Fig. 9 assist the reader to visualize the recirculating flow cells in the liquid phase (dark zone) due to natural convection. Because of the growing prominence of natural convection, PCM near the upper wall melted much faster than that in the lower part. Once the two aluminum fins were introduced, the shape of the melting interface changed drastically to a symmetric one as shown in Fig. 10. Two differences were observed, one of which was that melting was initiated on both the top and the bottom walls simultaneously with a nearly symmetric interface. The other difference was that due to the conductive nature of the fin, the PCM next to the insulated end wall started melting a little later than that next to the heated wall. The upper part of the interface remained very smooth due to the fact that the molten PCM was swept down the inclined interface by the convecting flow current. In contrast, however, it is remarkable that the lower part of the interface assumed a wavy shape due to its

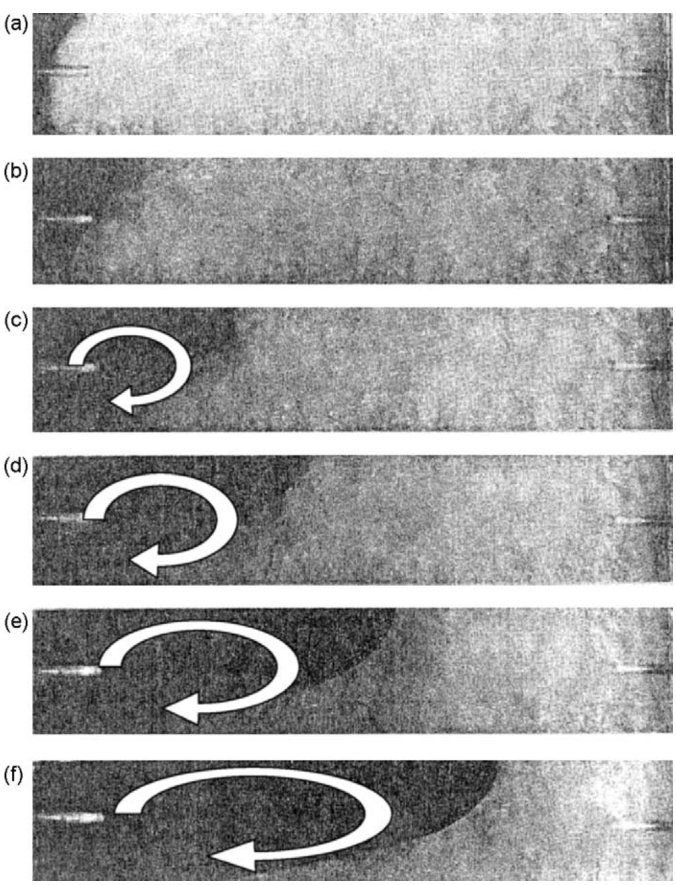


Fig. 9. Progress of the liquid–solid interface during melting for the case without fins (Henze and Humphrey [18]).

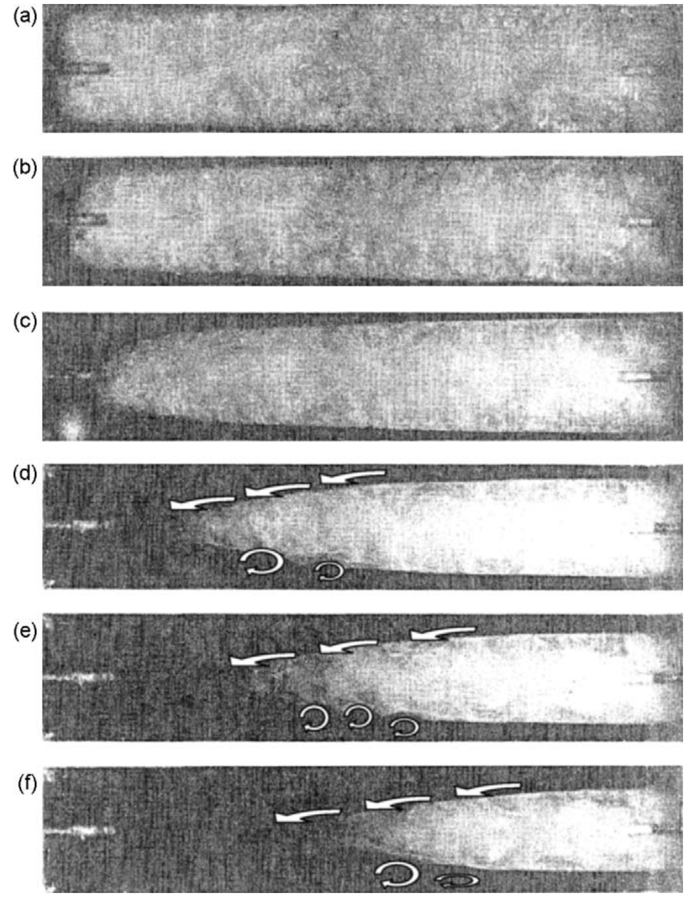


Fig. 10. Progress of the liquid–solid interface during melting for the case with fins of 3/32 inches thickness (Henze and Humphrey [18]).

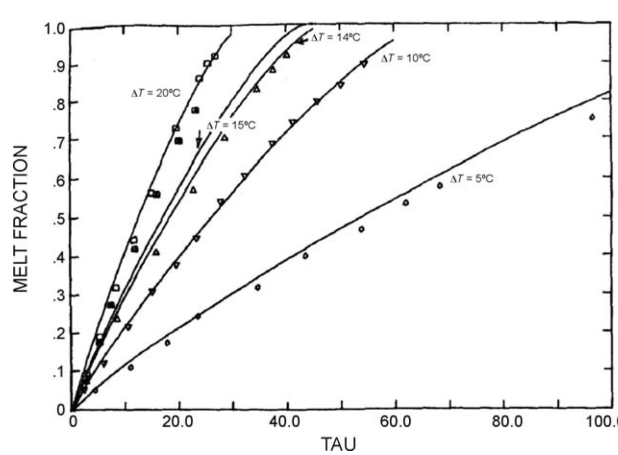


Fig. 11. Comparison of numerical predictions and experimental results for melt fraction versus time (Henze and Humphrey [18]).

interaction with the unstable Rayleigh-Benard convection cells. These are similar to "ice ripples" that were discussed by Epstein and Cheung [19]. Although some natural convection still exists in the case with fins, the heat transfer process was dominated by conduction promoted by the fin. The comparison between experimental data and the predictions of the model for the melt fraction, as plotted in Fig. 11, showed fairly good agreement, which indicates that the proposed model is applicable for this finned device. In general, the presence of metal fins significantly suppressed natural convection but strongly enhanced conduction. It was argued that if more fins are closely spaced, convection becomes more negligible and the proposed model can give better predictions.

Heat transfer enhancement of a paraffin wax thermal storage system by using metal fins was experimentally investigated by Eftekhar et al. [20] through flow visualization and analysis of the instantaneous interface position. A commercial paraffin wax (SUNTECH P116, that was a mixture of C_{20} through C_{32} hydrocarbons) with a melting point of about 317 K was selected as PCM. Some thermophysical properties of this paraffin wax were made available by the same authors earlier [21]. The dimensions of the rectangular thermal storage device were 53.5 mm (height) × 61.5 mm (length) × 56 mm (width). The device was divided into three identical sections by two vertically positioned plate fins. The front and back sides of the device were both covered by two Plexiglas layers each and an air gap between them. This allowed the flow inside each cell to be visually observed, and the top and bottom surfaces were both attached to constant-temperature water baths. The hot surface was set at the bottom wall and this might lead to flow instabilities. Experiments were conducted for different bottom-top temperature gradient combinations, which were 12.8, 17.6, 25.8, 27.6, and 33.8 °C. Convective circulating flow patterns during the melting process were clearly observed by the addition of red dye into the PCM, as shown in Fig. 12. The heated liquid next to the two fins of the cells rise vertically, thus replacing the colder fluid that sinks along the liquid–solid interface. Even though this arrangement is very similar to the cell utilized by Henze and Humphrey [18], the resulting flow patterns are different due to the difference in orientations of gravity and the fin. A symmetric melting pattern was observed by Eftekhar et al. [20], whereas Henze and Humphrey [18] reported waviness of the interface next to one of the fins due to presence of an unstable thermal layer. A sequence of photographs were taken [20] and digitized to determine the transient interface location at different time instants. A time-dependent bulk energy balance that used the information about the moving interface surface and the volume of the liquid phase was proposed to evaluate the effective convective heat transfer and the effective heat transfer coefficient as well. The dependence of the Nusselt number on the Rayleigh and Stefan numbers was also discussed.

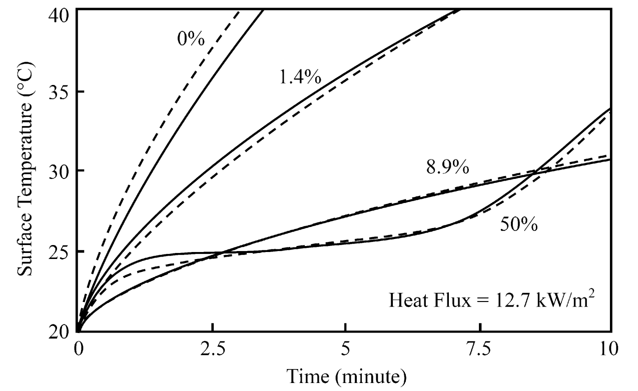


Fig. 13. Surface temperature versus time for different volume fractions (Knowles and Webb [22]).

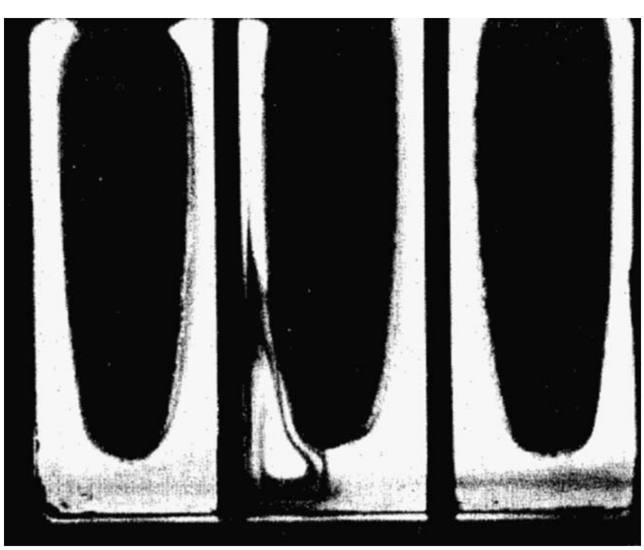


Fig. 12. Flow visualization of natural convection-induced recirculatory vortex (Eftekhar et al. [20]).

In order to address thermal management issues in relation to time-varying thermal loads that are encountered in spacecrafts, Knowles and Webb [22] proposed an idea of Metal/Phase Change Materials (M/PCM) composites. Such a material will take advantage of the high values of the thermal conductivity and specific heat of the metal and PCM components, respectively. Depending on the geometry, the metal component can be added in the form of plates, wires or fibers. In order to minimize thermal resistance, it was argued that the metal component should be distributed uniformly and aligned parallel to the desired direction of heat flow. Continuous conducting paths are preferred, so use of foams, sinters and randomly oriented wools are not optimum. "Fineness" of the metal component is an additional requirement so that little amount of PCM is unaffected by the heat front. By requiring that the thermal resistance along the conducting path must be greater than the resistance across the PCM layer, relations for maximum thicknesses of plates (sheets) or diameters of wires were developed for planar configurations. These dimensions must be maintained constant for planar cases, whereas for cylindrical and spherical cases, similar but distance-dependent relations can be derived. A

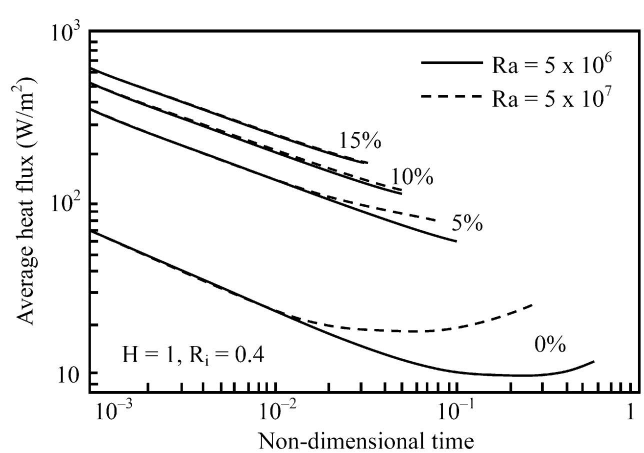


Fig. 14. Average heat flux at inner cylindrical wall versus time for different volume fractions of the metal matrix during melting (Tong et al. [24]).

simple one-dimensional unsteady model that ignored natural convection and sensible heat was derived for two limiting thermal conditions corresponding to incident heat flux and constant wall temperature cases. A test experiment was conducted using copper/dodecanol composites with four volumetric metal component concentrations of 0%, 1.4%, 8.9% and 50%. Copper foil strips, 5 cm wide and 0.025 cm thick, were coiled into a uniform spiral. The spiral fin was placed in a cylinder container with a cross-sectional diameter of 10 cm and a height of 5 cm. The container base was a 6 mm thick copper disk to which the spiral was soldered, whereas the remaining walls were made from lucite. It was mentioned that the PCM expanded 9% in volume during melting. The time-dependent surface temperature for the four volume fractions is presented in Fig. 13. The good agreement between the experimental data (symbols) and the numerical results (solid lines) indicates that the application of volume-averaged properties is valid since the two configuration requirements proposed before are satisfied in this experiment.

Chow et al. [23] proposed two techniques to enhance the thermal conductivity of LiH PCM that is usually used in high-temperature applications. The idea of the first enhancement technique was to use different shape of containers to encapsulate the LiH PCM. The interspaces filled with metal Li between the containers and the outer cylindrical capsule acted as enhanced heat conduction bridges. The second enhancement technique proposed a composite that consisted of metal Ni and LiH PCM. In this study, the metal Ni of 5% volume fraction within the PCM was investigated and the mixture was then encapsulated in a cylindrical capsule. The enhancement effects were numerically studied for two boundary conditions, which are constant surface heat flux and constant surface temperature. The results demonstrated that both techniques are apparently able to enhance the thermal conductivity of the original PCM but the composite approach gives the better effectiveness. They utilized a simple modeling approach in that the steady-state numerical simulation disregards convection effects. However, it showed clearly that the idea of using composite PCM might be an effective way to greatly enhance the thermal conductivity of original PCM.

Tong et al. [24] reported results of a numerical study on heat transfer within enhanced PCM by inserting an aluminum metal matrix in a cylindrical annulus. They studied both the diffusion and natural convection heat transfer effects during the melting and freezing processes utilizing separate transport equations for the two phases and coordinate transformations. The mixture of water/ice and the metal matrix was modeled as a saturated porous media by introducing the Darcy terms to the fluid's momentum equations. It must be mentioned that they considered the anomalous density variation of water in the phase change process and the ensuing dual counter-rotating vortex cells were clearly observed. The comparison of heat transfer enhancement for different volume fractions of the metal matrix as well as the effects of the Rayleigh number are shown in Fig. 14. Heat transfer

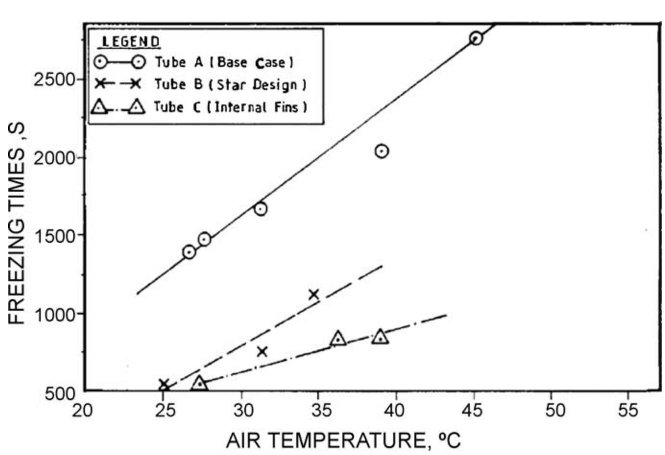


Fig. 15. Freezing times versus temperature for 6% volume fraction (Bugaje [25]).



Fig. 16. A photographic view of the lessing rings (Velraj et al. [28]).

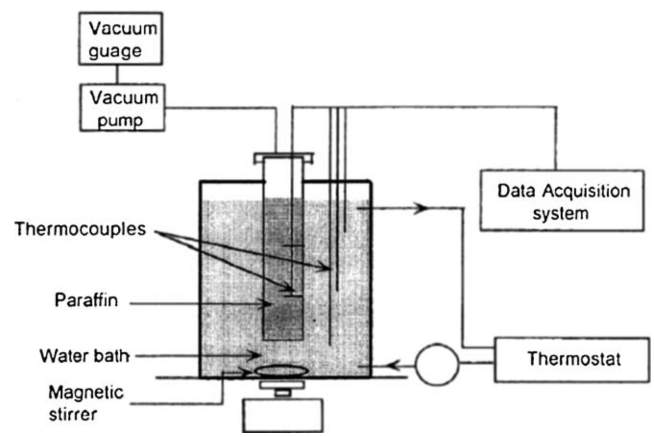


Fig. 17. Schematic diagram of the experimental setup (Velraj et al. [28]).

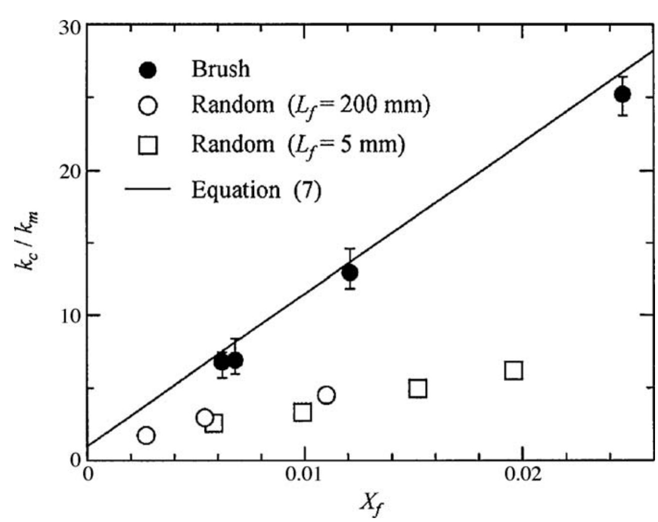


Fig. 18. Thermal conductivity enhancement of PCM using the brush type carbon fibers (Fukai et al. [30]).

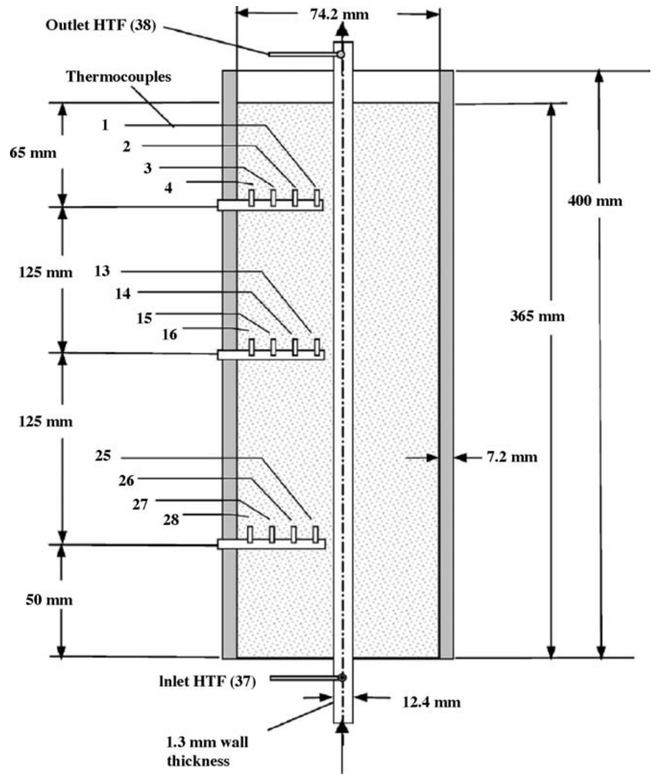


Fig. 19. Schematic diagram of the experimental setup with dimensions (Ettouney et al. [32]).

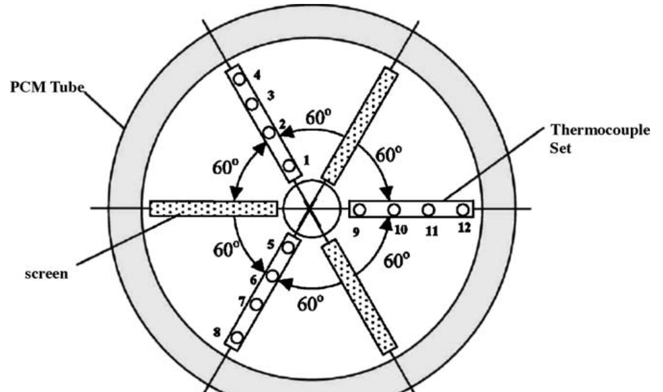


Fig. 20. Cross-section view of the annulus showing locations of metal screens with metal spheres and thermocouples (Ettouney et al. [32]).

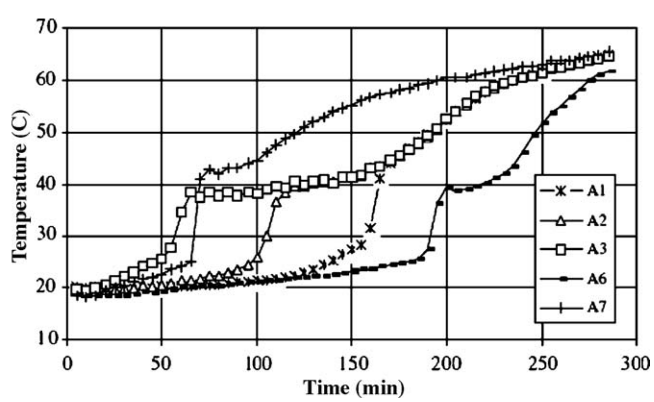


Fig. 21. Temperature variations versus time during melting process with fins (Stritih [33]).

enhancement is very marked for small volume fractions. However, further increase of the volume fraction does not enhance heat transfer linearly. They also pointed out the so-called undesirable "self-insulating" feature of PCM during the freezing process due to the growing thickness of the solidified material that acts as the insulator.

Bugaje [25] experimentally studied the enhancement of thermal response of a latent heat storage system. A paraffin wax and aluminum matrix were selected as the PCM and the promoter, respectively. An interesting aspect in this study was the utilization of plastic tubes to encapsulate the PCM. The effects of four kinds of matrices and two volume fractions on the thermal response were investigated and compared. Fig. 15 shows the variation of freezing times versus temperature for the volume fraction of 6%. The freezing times are shortened by a factor of 2 or greater for the two

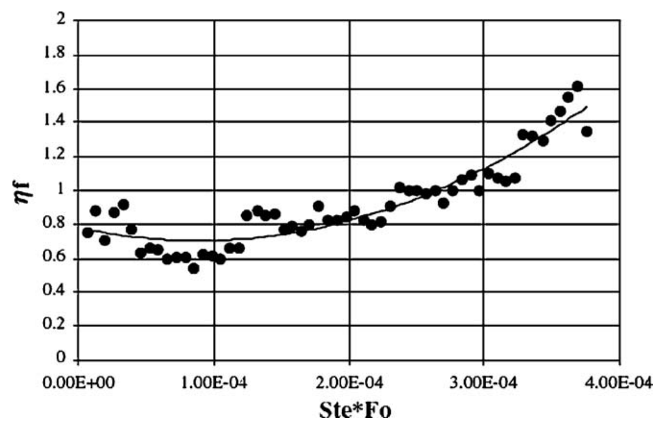


Fig. 22. Fin effectiveness versus dimensionless time during melting process (Stritih [33]).

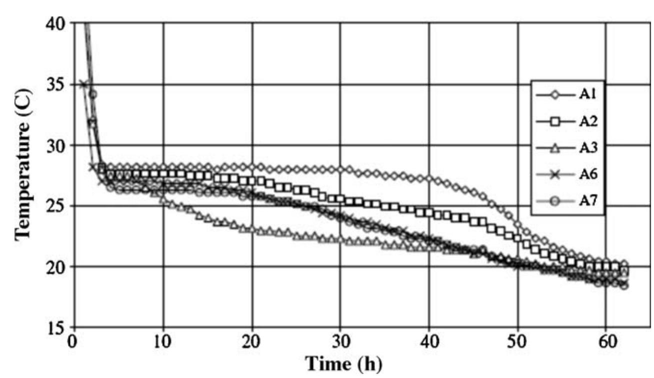


Fig. 23. Temperature variations versus time during solidification process with fins (Stritih [33]).

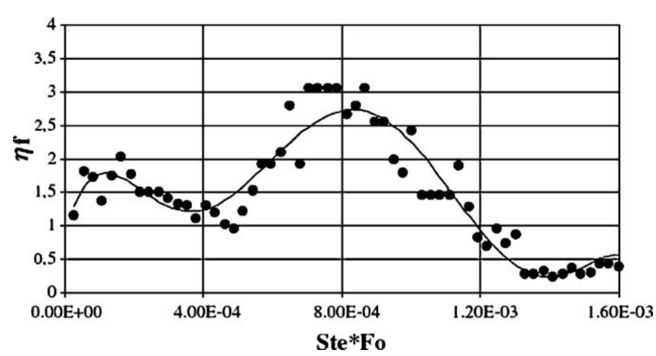


Fig. 24. Fin effectiveness versus dimensionless time during solidification process (Stritih [33]).

enhancement options that were used. The enhancement effects on freezing times were greater than that on melting times due to the "self-insulating" feature that implies the heat conduction plays a more significant role during the freezing processes. One shortcoming in this experimental study was the utilization of an air blower in a vertical column that was unable to guarantee an even heating on the outer surface of the tubes.

To examine the utilization of PCM for passive thermal control of avionics modules, Pal and Joshi [26] investigated the melting process within a honeycomb–PCM composite energy storage device, both experimentally and numerically. A honeycomb with a hexagonal cross-section was vertically installed inside a Plexiglas rectangular container. This assembly was then filled with *n*-triacontane that has a melting temperature of 338.6 K. The height of the honeycomb was 14.5 mm and each single cell of the honeycomb had a side wall thickness of 1.65 mm. Several T-type thermocouples were mounted at different positions inside the device to record the time-dependent temperature information. The device was designed to be heated from bottom by a silicone rubber patch heater. In the experiments, the power input was set from 15 to 60 W with increments of 5 W. A three-dimensional transient numerical simulation was carried out inside a single honeycomb cell that was simplified to one with an equivalent square cross-section with the same perimeter. Phase change was modeled using

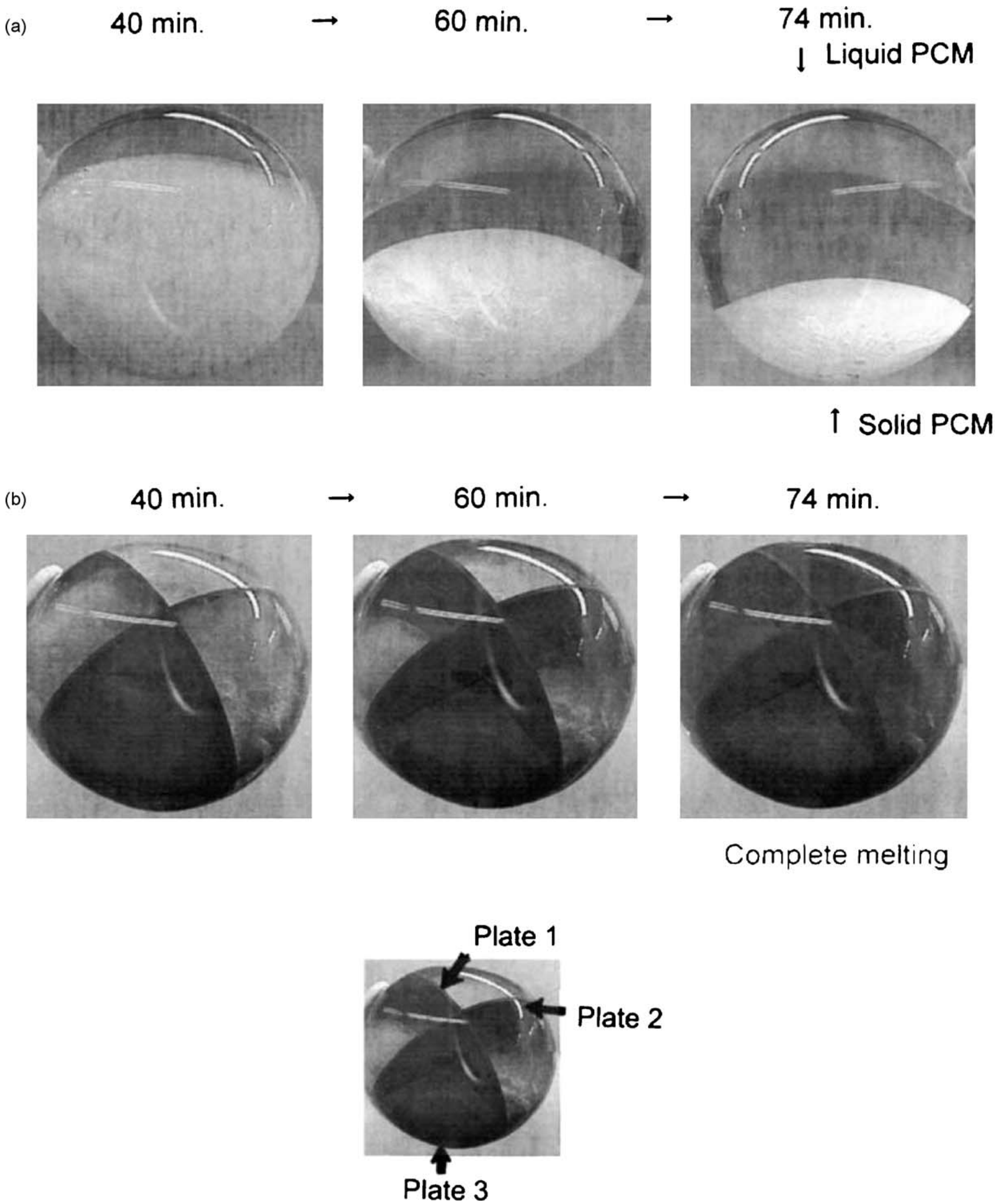


Fig. 25. Visualization of the melting process of solid PCM at $Re = 1800$. (a) Without copper plate and (b) with copper plates inserted (Koizumi [34]).

a widely used single-domain enthalpy-porosity technique, which was developed by Brent et al. [27]. Upon comparison between pure conduction and diffusion-convection-coupled simulations, natural convection was observed to be very weak and did not exhibit a noticeable effect on the shape of the melt interface. In view of substantial difference between predictions and measurements, the authors switched to a system-level modeling approach.

Velraj et al. [28] presented the utilization of three different heat transfer enhancement methods for a paraffin wax encapsulated in a cylindrical aluminum tube (6 cm outer diameter, 5.4 cm inner diameter and 60 cm long). The first approach was to use an internal longitudinal aluminum fin that had a cross-shaped cross-section. Secondly, the lessing rings with a diameter of 1 cm, which are shown in Fig. 16, were fully distributed inside the tube. The third method was employment of water/vapor bubbles that will randomly appear in the tube due to creating a low-pressure environment within a wax/water composite. The K-type NiCr–Ni thermocouples were utilized to measure the temperatures at different suitable locations inside the tube. As shown in Fig. 17, the experimental setup consisted of several parts, including a water bath with a magnetic stirrer and a thermostat, a data acquisition system, a vacuum pump, and so on. The operating procedure of the experiments was discussed in detail. They first employed the parameter estimation method to determine the outer heat transfer coefficient of the tube by comparing the measured data with the numerical results from an enthalpy-based model. Using the heat transfer coefficient, they further conducted both experimental and numerical work to predict the temperature variations versus time for the three approaches. The utilization of lessing rings of 20% volume fraction provided the best enhancement effect that significantly decreased the solidification time by a factor about 9. The enhancement effect of the internal fins with a volume fraction of 7% was a little lower, whereas loss of heat storage capacity for this method was much lower than the lessing rings option. They also found that the addition of water/vapor bubbles did not have a remarkable enhancement effect. The enhancing mechanism of the bubbles, which was not clearly discussed in this work, is very complicated and needs further studies.

Fukai et al. [29,30] used carbon fibers to enhance the thermal conductivity of a paraffin wax heat storage system. Carbon fibers were added to a paraffin to develop composite materials of two different types. In the first approach, randomly oriented fibers were utilized. The second method employed fiber brushes arranged along the radial direction of a cylindrical capsule. The volume fraction of carbon fibers for both types was restricted to less than 2%. They experimentally measured the transient temperature responses of both configurations of carbon fibers/paraffin composites using thermocouples. The thermal diffusivity of the composite was then determined via the nonlinear least squares parameter estimation technique. For the random-type composite, the fiber length only had a little effect on the enhancement of thermal conductivity. As the volume fraction of carbon fibers was raised, the thermal conductivity of the composite PCM also increased. As shown in Fig. 18, the effective thermal conductivity of the fiber brush composite was about three times greater than that of the random fiber composite because the heat flows along the fiber brush direction. This finding is in concert with the suggestions of Knowles and Webb [22] in relation to

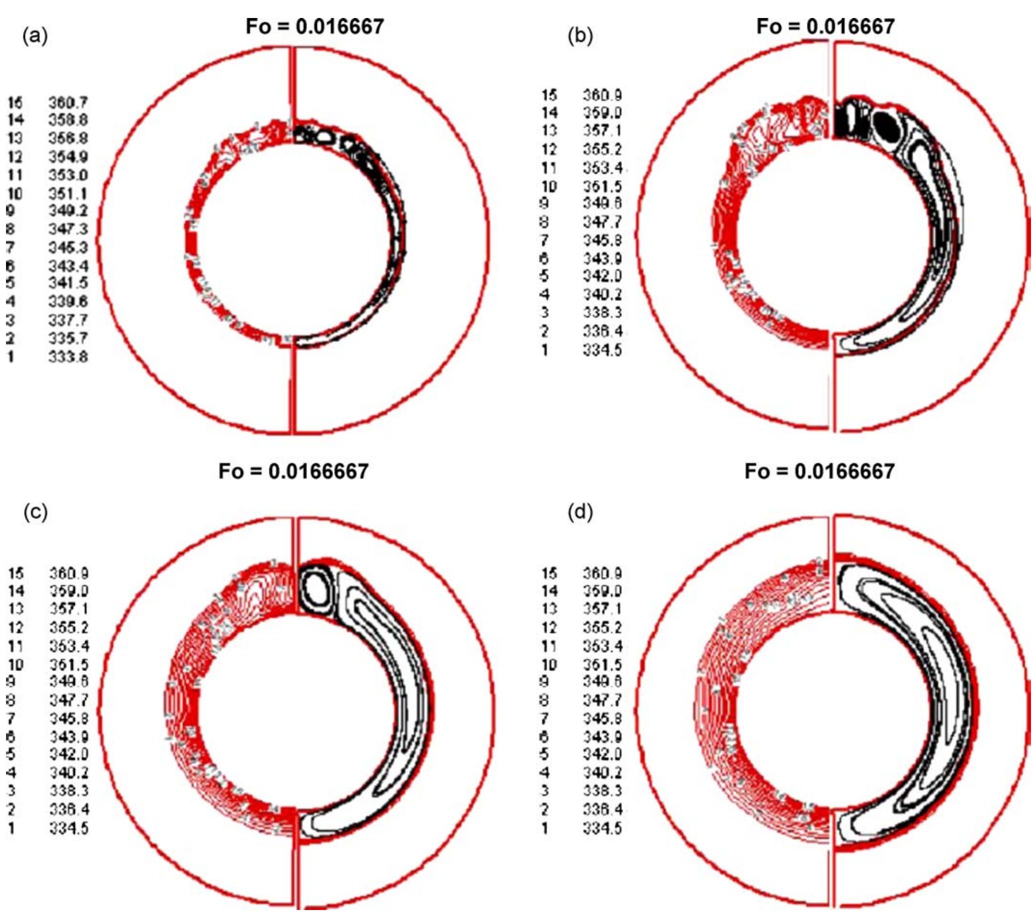


Fig. 26. Time-dependent temperature contours (left) and streamlines (right) for (a) pure PCM and porosity of (b) 0.95, (c) 0.90 and (d) 0.85 for $Ra = 10^7$, $Ste = 0.5$ and $k_s/k_f = 200$ (Mesalhy et al. [35]).

accommodating a minimum distance of the conducting media of the enhancers as opposed to utilization of randomly oriented media. The details on preparation of the stable fiber brush composite was not provided, which is really important in practical applications. Additionally, the measured data could have been analyzed better if natural heat convection was considered. For example, the estimation of the Grashof number will be helpful to the quantitative analysis of temperature variations during the melting and freezing processes.

Cabeza et al. [31] experimentally studied heat transfer enhancement of deionized water using three different kinds of promoters, which were stainless steel tube pieces, copper tube pieces, and graphite matrices. The experiments were carried out in a rectangular tank that was separated into two identical parts by an aluminum partition. This partition worked as both an intercooler and a heat exchanger. Six thermocouples were symmetrically mounted at different positions inside the tank. The signals from the thermocouples were recorded to investigate the moving times of the interface front during the melting and freezing processes. The volume fractions of the thermal conductivity enhancers for all three configurations were less than 10%. The results showed that the stainless steel tube pieces did not apparently enhance heat transfer. However, utilization of copper tube pieces and graphite matrices provided much better enhancement effects. It was noted that the melting and freezing times were significantly reduced by a factor up to 2.5. In this experiment, the middle partition of the tank provided a convenient way to simultaneously perform and compare the behaviors of two different enhancing techniques. However, an unavoidable drawback exists since the heat transferred through the two chambers is definitely unequal due to the differing heat transfer characteristics of both sides.

Ettouney et al. [32] carried out experiments on heat transfer enhancement for a paraffin wax within a cylindrical annulus. The metal screens and spheres made of stainless steel were selected as the enhancers. Spheres with three different diameters (8, 12, and 16 mm) as well as three different quantities (6, 12, and 24) were utilized. The volume fraction of the promoters was changed from 0.1% to 3.4%. As shown in Fig. 19, a total of 38 thermocouples, which were able to record detailed information about the temperature history at various positions were mounted at three different horizontal levels inside the annulus. Availability of these thermocouples also provided information on the progress of the interface during the melting process. In the experimental setup, three screens were radially positioned inside the annulus with uniform angular intervals and the spheres were attached to the screens. A cross-sectional view of the setup is presented in Fig. 20. Based on the experimental data, they investigated the variation of the Nusselt number as a function of temperature, the Stefan, Fourier and Rayleigh numbers, as well as the variation of the Fourier number as a function of temperature. The comparison among the results demonstrated that the metal spheres with a volume fraction of 2% led to the best enhancement effects. The employment of the dimensionless numbers was an effective approach to investigate the effectiveness of heat transfer enhancement. However, the exact definitions of some dimensionless numbers were not provided. For example, they did not specify how the characteristic lengths for the Nusselt number and the Rayleigh number were chosen.

Stritih [33] conducted an experimental study of enhanced heat transfer of a rectangular PCM thermal storage system with dimensions of 650 mm × 500 mm × 120 mm. This shape of storage system is usually used as the storage wall for buildings. Commercial RT 30 paraffin with a melting temperature of about 306 K was used because it is proper for thermal comfort in building applications. On one of the 650 mm × 500 mm side walls, a rectangular water heat exchanger was placed for heating or cooling. The remaining five side walls were insulated by polystyrene layers with an extremely small thermal conductivity of 0.038 W/mK. Thus, the boundary conditions on these walls can be treated as adiabatic. Thirty-two steel fins with a thermal conductivity of 20 W/mK were evenly spaced in the rectangular chamber. Dimensions for the fins were height of 0.5 m, length of 0.12 m and thickness of 1 mm. The volume fraction of the fins was then determined to be approximately 0.5% based on the geometry relationship. Five thermocouples were mounted at different positions inside the chamber. An uncertainty analysis showed that the uncertainty for the heat flux measurement was within ±1.35%. Fig. 21 shows the temperature variations versus time during the melting process with fins. In comparison to similar measurements without fins, the transition time for the case with fins was a little longer. This indicates that the addition of fins did not have the desired effects on heat transfer enhancement of the system during the melting process. The reason would be that natural convection was significantly suppressed by the fins due to a lower Rayleigh number but the compensation from heat conduction enhancement was not great enough. Several dimensionless parameters, like the Nusselt and Rayleigh numbers, were defined to assist the analysis of phase change heat transfer processes. However, the values of the Rayleigh numbers with or without fins, which are convenient measures of the intensity of heat convection, were not provided. If the Rayleigh numbers were specified, the comparison of heat convection effect would become much more straightforward. In addition, the ratio of heat transfer with fins to that without fins was referred to as the fin effectiveness. For the melting process, the fin effectiveness versus a dimensionless time $Ste \times Fo$ was sketched (Fig. 22). This diagram shows that for a time duration at the beginning, the fin effectiveness was less than unity, which means that the heat transfer with fins was lower than that without fins. This confirmed the significance of heat convection during the melting process. In contrast, however, for the freezing process, heat convection is much less important and heat conduction becomes dominant. The temperature variations versus time during the solidification process with fins are shown in Fig. 23. As expected, the moving of the interface front was much faster than for the case without fins. The enhancement effect can be demonstrated via the fin effectiveness diagram that is shown in Fig. 24. For a long time duration, the fin effectiveness was much greater than unity up to a maximum of 3.06. It is obvious that heat transfer was greatly enhanced by the presence of high thermal-conductivity fins during the solidification process.

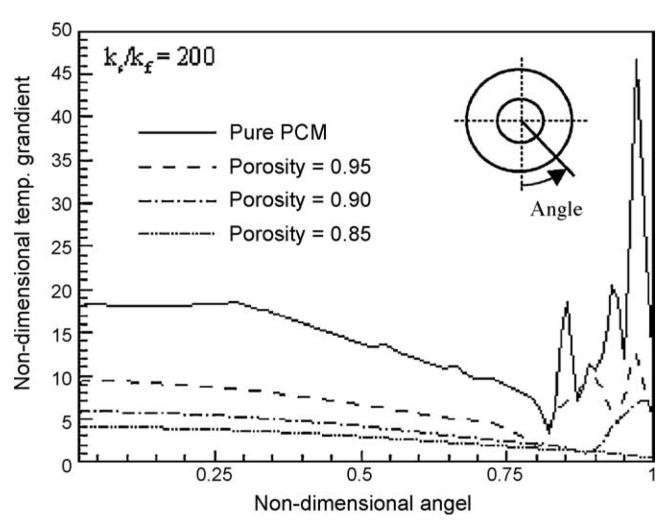


Fig. 27. Dimensionless PCM phase temperature gradient on the inner surface of the cylinder for $Ra = 10^7$, $Ste = 0.5$, $Fo = 0.016667$ and $k_s/k_f = 200$ (Mesalhy et al. [35]).

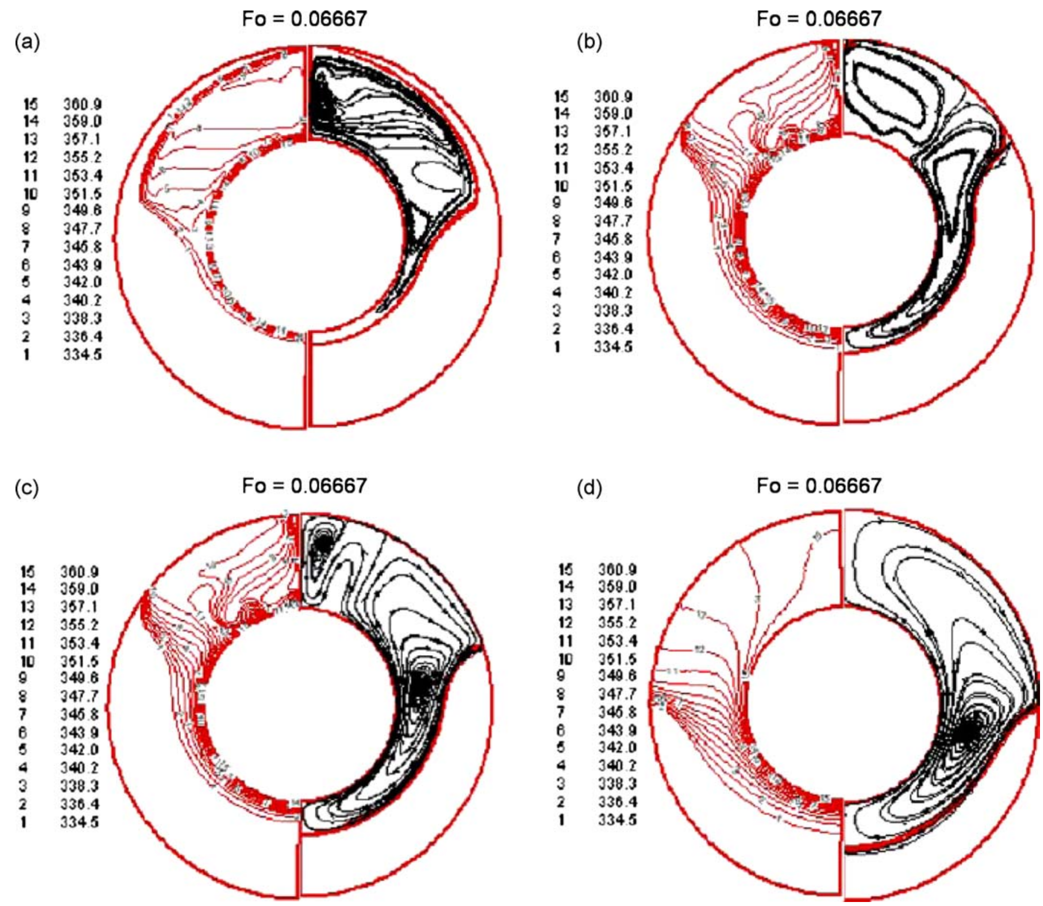


Fig. 28. Time-dependent temperature contours (left) and streamlines (right) for (a) pure PCM and conductivity ratio of (b) 50, (c) 100 and (d) 200 for $Ra = 10^7$, $Ste = 0.5$ and porosity of 0.90 (Mesalhy et al. [35]).

By providing visualization photographs, Koizumi [34] communicated results of an experimental study of unconstrained (also known as unfixed) melting of *n*-octadecane that was contained within spherical capsules. The glass capsules that had an outer diameter of 50 mm and wall thickness of 1 mm, were placed in a controlled heated air flow stream. Of relevance to this review were a set of experiments during which three copper plates were placed inside the capsule, as shown in Fig. 25. Due to presence of these copper plates that were intersecting each other at 90°, the observed melting period was reduced by 29–33%, the extent of which depended on the prevailing Reynolds number for external flow over the sphere.

Mesalhy et al. [35] numerically studied the melting process of PCM inside a cylindrical annulus. A solid porous matrix with high conductivity and high porosity, which filled the annulus, was saturated with a generic PCM. The matrix was assumed to be made up of repeating rectangular cells with conductive fibers being the sides of the cell. The convective motion of liquid phase PCM in porous domain was investigated by introducing the Darcy, Brinkman and Forchiermer terms to the momentum equations.

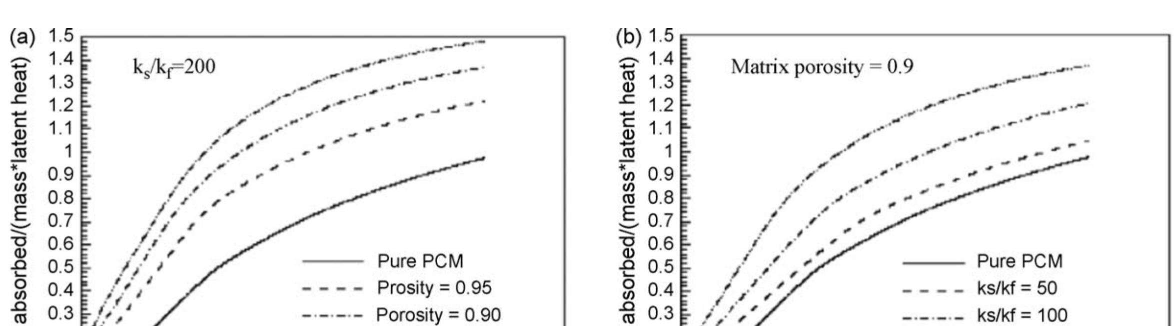


Fig. 29. The absorbed heat as a function of the Fourier number for (a) different porosities and (b) different thermal conductivity ratios (Mesalhy et al. [35]).

The widely used finite-volume technique was employed to solve the volume-averaged transport equations. However, unlike most previous studies, the main contribution in this paper was consideration of local thermal non-equilibrium between the solid matrix and the PCM by using two coupled energy equations. The two energy equations were coupled through an interfacial heat transfer coefficient between the solid matrix and the PCM. This quantity was determined using a quasi-steady heat diffusion analysis between the porous matrix and the PCM. Effective thermal conductivities of the two energy equations were estimated using the matrix model described above. A parametric study was performed to observe and compare the effects on the thermal response of the storage system by changing the matrix porosity and the ratio of thermal conductivity between the solid matrix and the PCM with $Ra = 10^7$ and $Ste = 0.5$. With the thermal conductivity ratio equal to 200, the temperature distributions and streamlines for a pure PCM without matrix and three different matrix porosities of 0.95, 0.9, and 0.85 at dimensionless time instant $Fo = 0.016667$ are presented in Fig. 26. Despite the damping of convective motion of liquid phase PCM upon decreasing the matrix porosity, the melting rate still increased due to the significant enhancement of the effective thermal conductivity of the PCM/matrix mixture. As shown in Fig. 27, fluctuation of dimensionless surface temperature gradient occurred due to the flow separation that appeared in the upper region of the inner cylinder. This flow separation phenomenon is shown clearly in Fig. 26. It is also noted that the pure PCM without the matrix exhibited the most intensive separation and temperature gradient fluctuations. As the matrix porosity was decreased, the temperature gradient fluctuations became weak. For a porosity of 0.85, the fluctuations almost disappeared. For the matrix porosity of 0.9, the temperature variations and streamlines for a pure PCM and three different conductivity ratios of 50, 100 and 200 at dimensionless time instant $Fo = 0.06667$ are plotted in Fig. 28. The melting rate increased as the thermal conductivity of the solid matrix was raised, especially in the lower region of the cylinder. For a pure PCM (Fig. 28a), melting and ensuring convection is favored in the upper half of the annulus, that is very similar to results of Khodadadi and Zhang [36]. Increasing the thermal conductivity ratio gave rise to faster melting in the lower part of the annulus and emergence of multi-vortex recirculating structures and their mergings. It was also demonstrated that both the increases of matrix porosity and thermal conductivity ratio greatly enhanced heat absorption, as shown in Fig. 29. It is observed that the time duration for heat absorption can be lowered significantly by increasing the thermal conductivity of solid matrix or lowering the porosity. This study is a good example of application of a model for solving the transient phase change problem inside a porous domain. In the absence of a segregated but coupled solution that requires meshing of different phases, this approach is a good contribution to design of practical thermal storage problems.

Ettouney et al. [37] performed both melting and solidification experiments of commercial grade paraffin wax within spherical capsules that also contained metallic beads. The copper spherical

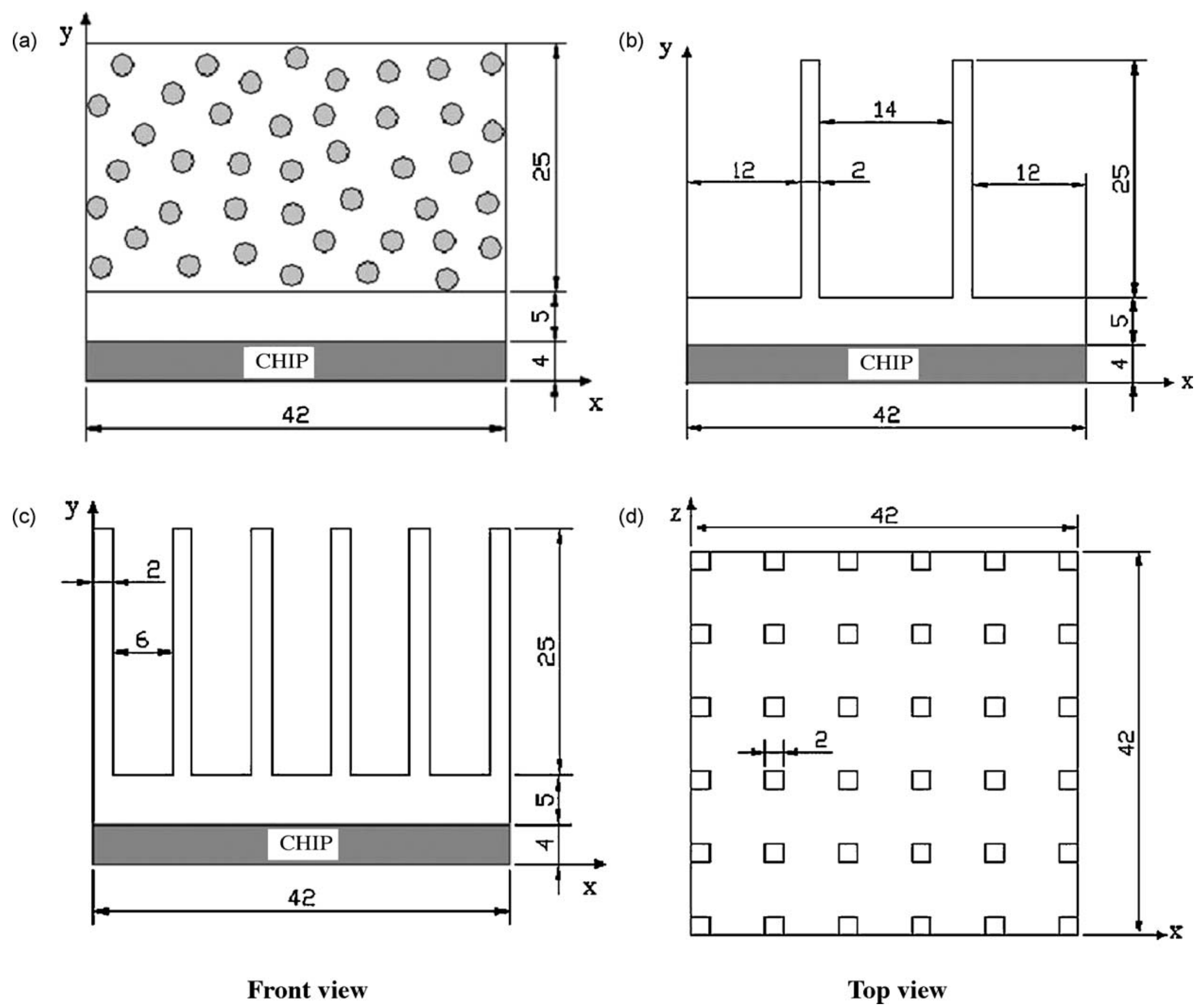


Fig. 30. Arrangements and dimensions in millimeters for three kinds of PCM/enhancer combinations of (a) matrix, (b) plate-type fins and (c) rod-type fins (Nayak et al. [38]).

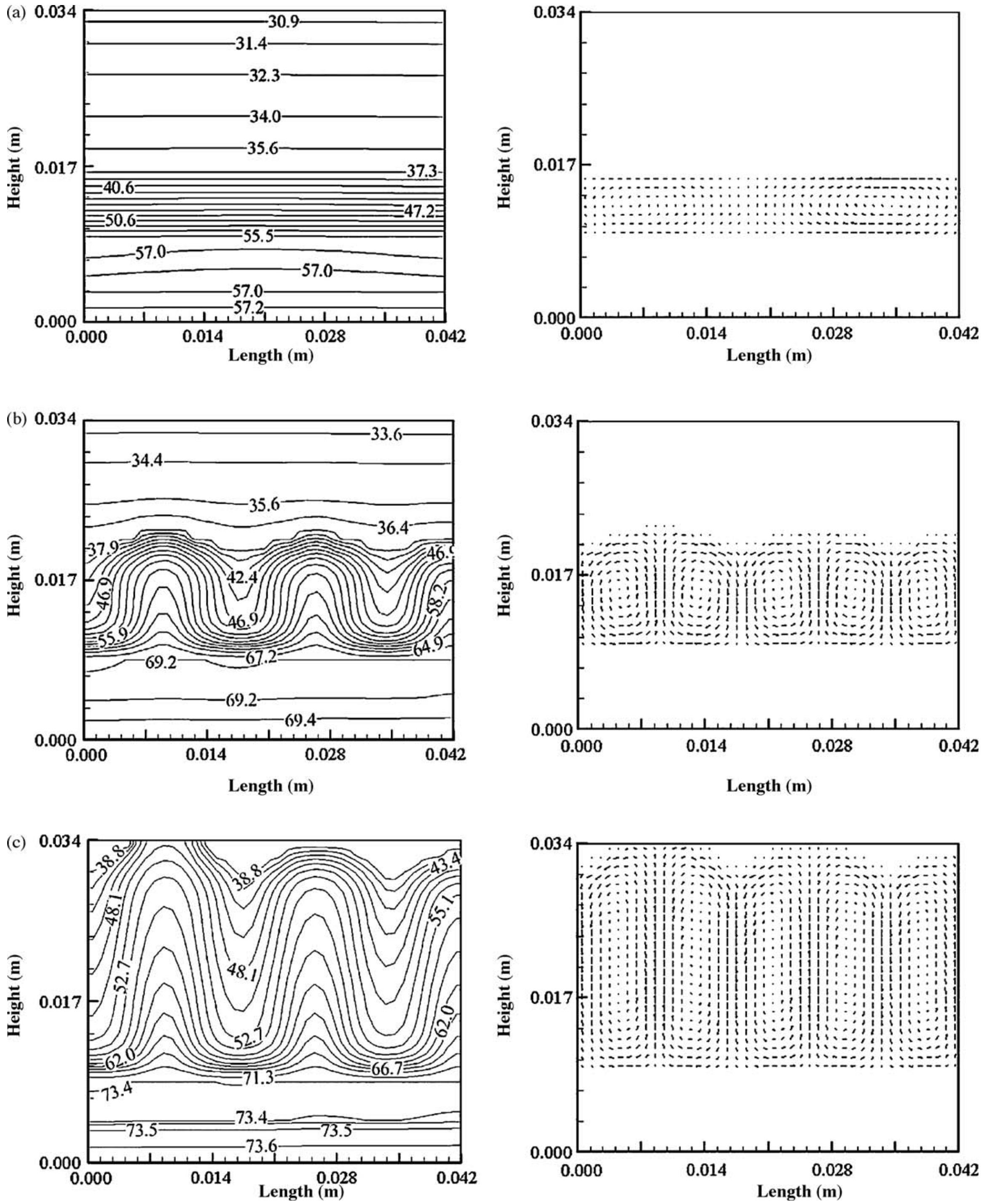


Fig. 31. Temperature and velocity distributions for the matrix option at three time instants of (a) 2100 s, (b) 2700 s and (c) 3600 s with porosity = 0.85, $Da = 4.74 \times 10^{-5}$ and chip power = 4 W (Nayak et al. [38]).

capsule had outer diameter and wall thickness of 3 and 0.1 cm, respectively. The stainless steel spherical beads had diameters of 4, 5 and 6 mm and the volume ratio of the beads within the capsule ranged between 0.5 and 20%. The capsule was instrumented with 10 thermocouples placed along two axes normal to each other. The capsule was heated or cooled by an air stream flowing vertically upward within a tube. No flow visualization photos were possible in this arrangement and liquid–solid interfaces could only be inferred from the thermocouple readings. Reductions as high as of 13% for the melting and solidification times were reported. The main advantage of this scheme has to do with the ability of the metal beads to rearrange on the bottom of the sphere upon possible tumbling of the spherical storage system. On the other hand, the metal beads will clearly weaken convection within the space among them that otherwise is expected to be the site of intense melting. In addition, the packing of the beads will not necessarily give rise to a minimum thermal resistance path. These shortcomings are reflected in the modest gains for the system.

Nayak et al. [38] developed a numerical model to study the effects of the utilization of PCM with thermal conductivity enhancers on the heat transfer performance of a heat sink used for cooling of electronics. Eicosane with a melting temperature of

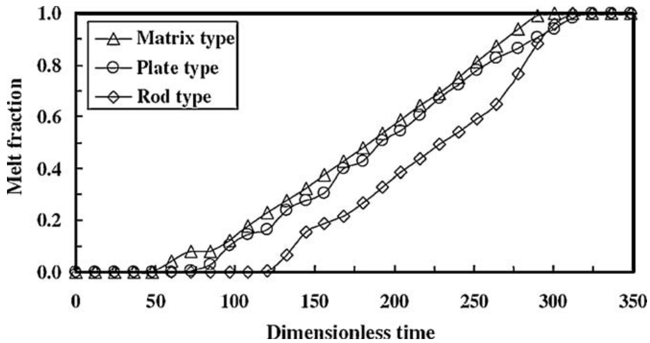


Fig. 32. Comparison of melting fraction versus time for three options (Nayak et al. [38]).

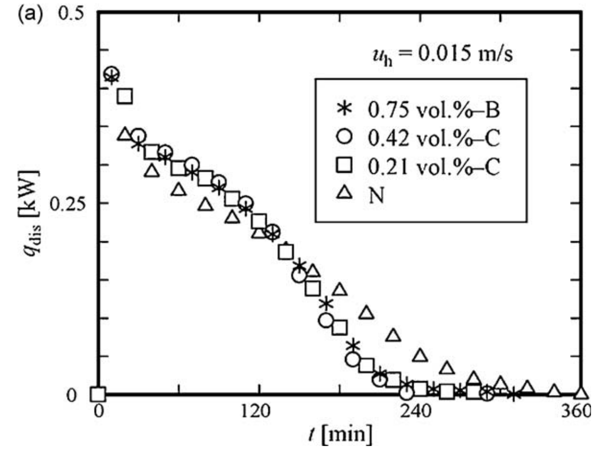


Fig. 34. Comparison of thermal energy retrieval rates for different volume fraction and installation option of carbon fibers under a constant flow rate (Nakaso et al. [39]).

310 K, as well as aluminum with a high thermal conductivity of about 180 W/mK were selected as the PCM and enhancer material, respectively. The heat sink with three different kinds of PCM/enhancer combinations are schematically sketched in Fig. 30. Dimensions of the heat sink, heat-generating chip and the rectangular cavity located upon the heat sink, which was filled with the PCM and aluminum matrix or fins, were also specified in Fig. 30. For the case of the aluminum porous matrix, a local thermal equilibrium model and the volume-averaging technique were employed. The thermal conductivity used in the energy equation was the effective thermal conductivity of the PCM/aluminum matrix evaluated by a well-established model. The transient phase change effect was simulated by the single-domain enthalpy-porosity approach with the solid-liquid interface assumed to be a mushy region. The computational procedures were presented in detail for both matrix and fins configurations. Some useful dimensionless variables were also defined to assist the heat transfer analysis. The temperature and velocity distributions for the matrix option at two different instants are shown in Fig. 31. Soon after melting of the PCM starts, heat conduction was dominant, which was indicated by the parallel lines of the temperature contours shown in Fig. 31(a). With further progress of melting, natural convection became more important. At a time instant of 3600s near completion of melting, as shown in Fig. 31(c), the flow pattern inside the cavity illustrated several recirculating cells in the region of melted PCM that is usually referred to as the Rayleigh-Benard convection cells. A parametric study was then conducted by varying in turn the Darcy number and the volume fraction of the matrix. The results showed that as the volume fraction was increased, natural convection was suppressed. This gives rise to a negative effect on the uniformity of temperature inside the cavity, which is very important for cooling of electronics. It was also concluded that for the same value of the volume fraction of the thermal conductivity enhancer, the cooling performance was improved for a bigger size of the matrix. Similar parametric studies were also presented for the two fins options except for adding one more parameter of the chip power. The three-dimensional study on the rod-type fins option showed clearly that it exhibited the best temperature uniformity, which gave almost uniform temperature variation inside the entire domain. The melting fraction versus dimensionless time for the three options are compared in Fig. 32. The comparison among the options revealed that for the rod-type fin option, the starting of melting was delayed. However, despite a delay at the beginning, the rod-type option exhibited a faster melting rate.

Nakaso et al. [39] conducted an experimental study to explore the effectiveness of using carbon fiber cloths to provide extended heat exchange area and enhanced thermal conductivity for a latent heat thermal energy storage unit. Woven carbon fiber cloths of

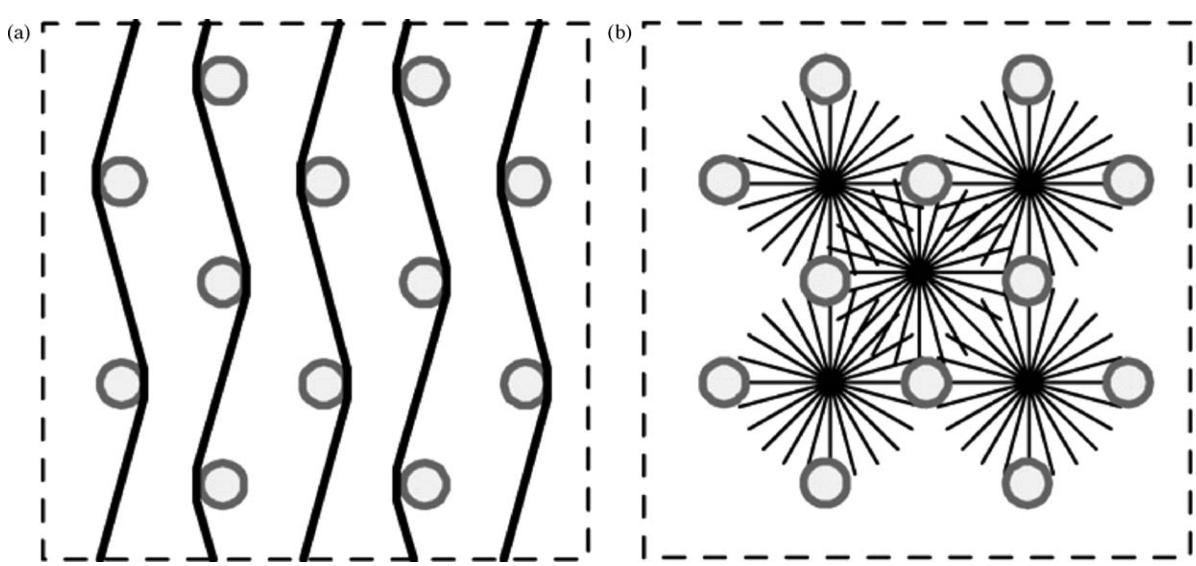


Fig. 33. Schematic diagrams of two different installation options: (a) cloths and (b) brushes of carbon fibers in a thermal energy storage tank (Nakaso et al. [39]).

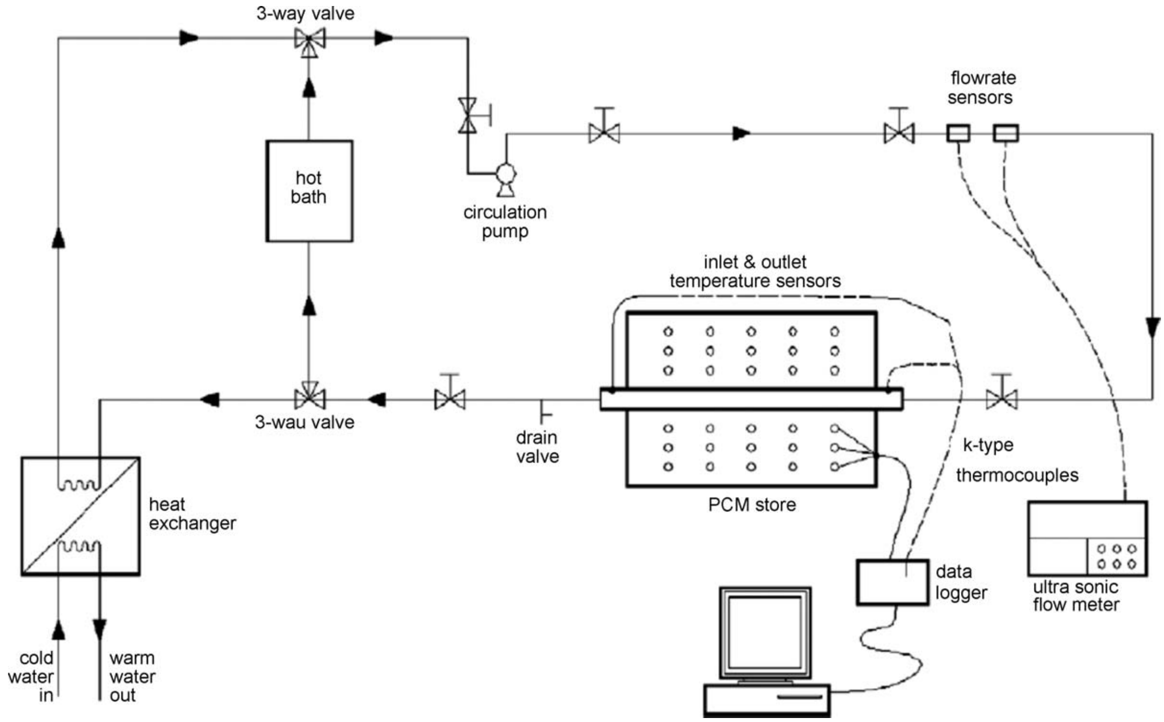


Fig. 35. Schematic diagram of the experimental set-up of PCM stored in a concentric tube with circular or longitudinal fins (Agyenim et al. [40]).

surface densities equal to 142 and 304 g/m^2 were laid in contact with the copper tubes (inner and outer diameters of 8 and 9.5 mm, respectively) of a shell-and-tube type heat exchanger (shown in the left diagram of Fig. 33). The actual volume fractions were 0.42 and 0.83%, however the authors claimed that fibers laid parallel to the copper tubes did not affect heat transfer. Thus, the reported volume fractions were 0.21 and 0.42%. Carbon fiber bushes (similar to Fukai et al. [29,30]) were also explored as an alternative arrangement with a volume fraction of 0.75% (diagram on the right side of Fig. 33). Commercial paraffin wax was then introduced into the space surrounding the copper tubes and the conductivity enhancing medium. Ignoring convective heat transfer in the liquid phase, a transient 3-D conduction formulation of the system was adopted. The model accounted for the effective heat capacity of the PCM/carbon fiber composite including the effect of the latent heat of the PCM. A non-isotropic thermal conductivity tensor was also utilized. Utilizing measurements of the inlet and outlet fluid temperatures of the heat exchanger, heat transfer rates during energy discharge for various thermal conductivity enhancement combinations for a constant flow condition are given in Fig. 34. The system utilizing carbon fiber cloth with a volume fraction of 0.42% exhibits a shorter discharge time of the order of 20%.

Agyenim et al. [40] reported on the performance of circular and longitudinal copper fins utilized as thermal conductivity promoters within a horizontal concentric tube heat exchanger containing Erythritol as the PCM (Fig. 35). The storage container for the PCM was an aluminum cylinder 1 m long, inside diameter of 146.4 mm and a wall thickness of 3 mm. The two ends of the storage container were sealed using 3 mm thick aluminum plates. A copper tube with a diameter of 54 mm was positioned concentrically in the storage container. Two flow loops were utilized for passing the appropriate heat transfer fluid through the container. These working fluids were silicone oil during 8 h of charging (melting of the PCM) and water during discharging of energy. One mm thick copper plates were utilized as radial fins (8 equally spaced fins 0.125 m apart) and longitudinal (8 equally spaced circumferentially). For both types of fins, a 3 mm gap was allowed between the tip of the fins and the container of the PCM (Fig. 36). The contact surface areas of the copper tube/fin and PCM were 0.1697, 0.3587 and 0.7777 m^2 for the control, circular fin and longitudinal fin systems, respectively. Glass wool insulation (thickness of 100 mm and thermal conductivity of 0.04 W/mK) was wrapped around the container to minimize heat exchange with the atmosphere. Consecutive thermal cycling of a small sample of Erythritol using

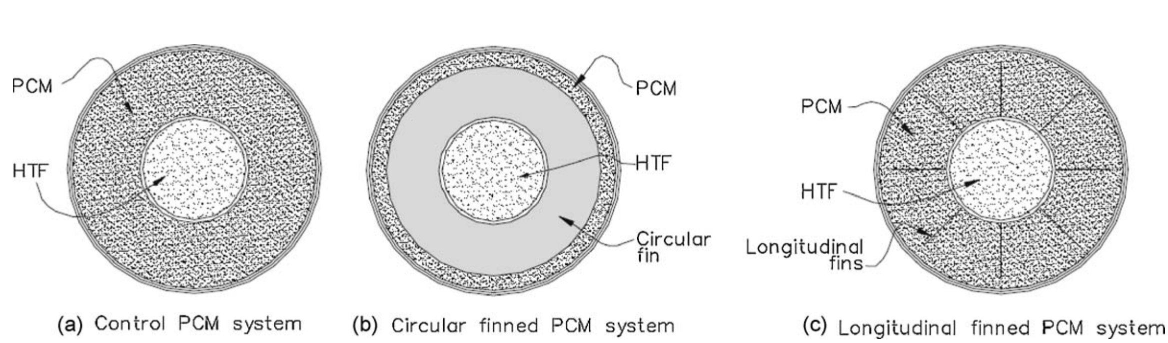


Fig. 36. Schematic diagrams of the cross-sectional areas of the (a) control system without fins, (b) circular fin, and (c) longitudinal fin systems (Agyenim et al. [40]).

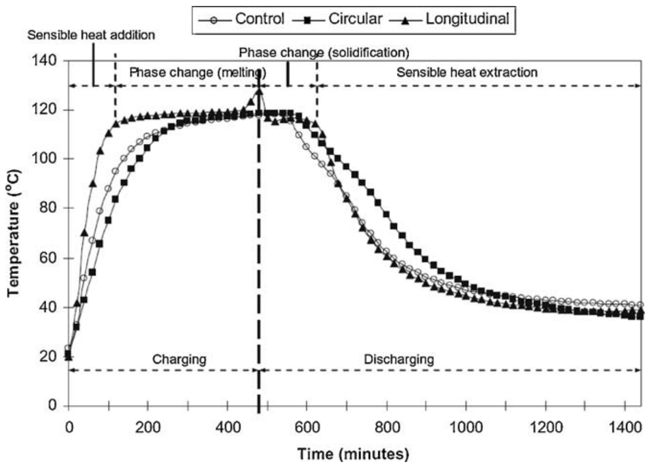


Fig. 37. Comparison of the transient average temperature in the PCM tube for the control, circular fin, and longitudinal fin systems for both charging and discharging processes (Agyenim et al. [40]).

DSC for the temperature range of 20–140 °C (±2 °C) was conducted. The values of heat of fusion and melting temperature showed sensitivity to the number of cycles (maximum of 20). Forty K-type thermocouples were placed at 5 axial stations and various circumferential stations in order to monitor the thermal field and check on the axisymmetry of the system. Transient values of the average temperature within the container during the charge and discharge of energy are shown in Fig. 37. During the charging process, the average temperature for the longitudinal system was consistently higher than the values for the control and circular fin systems. The storage efficiencies of three systems were compared and the longitudinal fin system exhibited to be a system that was capable of storing the greatest amount of energy.

5. Concluding remarks

A review of experimental/computational work to promote the thermal conductivity of PCM was presented. The original impetus is shown to be the thermal management of electronics for aeronautics and space exploration, followed by subsequent extension to storage of thermal energy for solar thermal applications. Focusing on placement of *fixed, stationary* high conductivity inserts, the thermal conductivity promoter materials have been copper, aluminum, nickel, stainless steel and carbon fiber in various forms (fins, honeycomb, wool, brush, etc.). The reviewed research work encompassed a variety of PCM, operating conditions, heat exchange and thermal energy storage arrangements. These included isolated thermal storage units (rectangular boxes, cylinders and spheres) and containers that exchange energy to a moving fluid medium passing through it. At times, research has focused on the significant role of flow regimes that are created due to the presence of thermally unstable fluid layers that lead to enhanced convective mixing and thus expedited melting of PCM. Parallel to this, it was shown that due to utilization of fixed high conductivity inserts, the conducting pathways connecting the hot and cold ends must be minimized.

Acknowledgements

This material is based upon work partially supported by the US Department of Energy under Award Number DE-SC0002470. The first author also acknowledges financial support provided by the Alabama EPSCoR Program under the Graduate Research Scholars Program (Round 5).

References

[1] Abhat A. Low temperature latent heat thermal energy storage-heat storage materials. Solar Energy 1983;30:313–32.
[2] Kamimoto M. Thermal energy storage technology. International Journal of Solar Energy 1987;5:21–33.
[3] Hasnain SM. Review on sustainable thermal energy storage technologies, Part I: Heat storage materials and techniques. Energy Conversion and Management 1998;39:1127–38.
[4] Zalba B, Marin JM, Cabeza LF, Mehling H. Review on thermal energy storage with phase change: materials, heat transfer analysis and applications. Applied Thermal Engineering 2003;23:251–83.
[5] Farid MM, Khudhair AM, Razack SAK, Al-Hallaj S. A review on phase change energy storage: material and applications. Energy Conversion and Management 2004;45:1597–615.
[6] Sharma SD, Sagara K. Latent heat storage materials and systems: a review. International Journal of Green Energy 2005;2:1–56.
[7] Kenisarin M, Mahkamov K. Solar energy storage using phase change materials. Renewable and Sustainable Energy Reviews 2007;11:1913–65.
[8] Regin AF, Solanki SC, Saini JS. Heat transfer characteristics of thermal energy storage system using PCM capsules: a review. Renewable and Sustainable Energy Reviews 2008;12:2438–58.
[9] Jegadheeswaran S, Pohekar SD. Performance enhancement in latent heat thermal storage system: a review. Renewable and Sustainable Energy Reviews 2009;13:2225–44.
[10] Humphries WR, Griggs EI. A design handbook for phase change thermal control and energy storage devices. NASA Technical paper 1074 1977;256.
[11] Bentilla EW, Sterrett KF, Karre LE. Research and development study on thermal control by use of fusible materials. Northrop Space Laboratories Interim Report (NSL-65-16-1). NASA Marshall Space Flight Center; 1966, 179 pp.
[12] Hoover MJ, Grodzka PG, O'Neill MJ. Space thermal control development. Lockheed Huntsville Research and Engineering Center Final Report, LMSC-HREC D225500; 1971, 81 pp.
[13] Humphries WR, Performance of finned thermal capacitors. NASA Technical Note D-7690; 1974, 340 pp.
[14] Griggs EI, Pitts DR, Humphries WR. Transient analysis of a thermal storage unit involving a phase change material, paper 74-WA/HT-21. In: ASME Winter Annual Meeting; 1974.p. 9.
[15] Abhat A. Experimental investigation and analysis of a honeycomb-packed phase change material device. In: AIAA 11th Thermophysics Conference; 1976.p. 9 (Paper AIAA-76-437).
[16] De Jong AG, Hoogendoorn CJ. Improvement of heat transport in paraffins for latent heat storage systems, in thermal storage of solar energy. In: Proceedings of an International TNO—Symposium. Amsterdam, The Netherlands: Martinus Nijhoff Publishers; 1981. p. 123–33.
[17] Abhat A, Aboul-Enein S, Malatidis NA. Heat-of-fusion storage systems for solar heating applications. In: Thermal storage of solar energy, Proceedings of an International TNO—Symposium. Amsterdam, The Netherlands: Martinus Nijhoff Publishers; 1981. p. 157–71.
[18] Henze HR, Humphrey JAC. Enhanced heat conduction in phase-change thermal energy storage devices. International Journal of Heat and Mass Transfer 1981;24:459–74.
[19] Epstein M, Cheung FB. Complex freezing–melting interfaces in fluid flow. Annual Review of Fluid Mechanics 1983;15:293–319.
[20] Eftekhar J, Haji-Sheikh A, Lou DYS. Heat transfer enhancement in a paraffin wax thermal storage system. Journal of Solar Energy Engineering 1984;106:299–306.
[21] Haji-Sheikh A, Eftekhar J, Lou DYS, Some thermophysical properties of paraffin wax as a thermal storage medium. Spacecraft Thermal Control, Design, and Operation, vol. 86. Progress in Astronautics and Aeronautics. AIAA, New York, New York; 1983, p. 241–53.
[22] Knowles TR, Webb GW. M/PCM composite thermal storage materials. In: AIAA 22nd Thermophysics Conference; 1987.p. 6 (Paper AIAA-87-1489).
[23] Chow LC, Zhong JK, Beam JE. Thermal conductivity enhancement for phase change storage media. International Communications in Heat and Mass Transfer 1996;23:91–100.
[24] Tong X, Khan JA, Amin MR. Enhancement of heat transfer by inserting a metal matrix into a phase change material. Numerical Heat Transfer Part A 1996;30:125–41.
[25] Bugaje IM. Enhancing the thermal response of latent heat storage system. International Journal of Energy Research 1997;21:759–66.
[26] Pal D, Joshi YK. Thermal management of an avionics module using solid-liquid phase-change materials. Journal of Thermophysics and Heat Transfer 1998;12:256–62.
[27] Brent AD, Voller VR, Reid KJ. Enthalpy-porosity technique for modeling convection-diffusion phase change: application to the melting of a pure metal. Numerical Heat Transfer 1988;13:297–318.
[28] Velraj R, Seeniraj RV, Hafner B, Faber C, Schwarzer K. Heat transfer enhancement in a latent heat storage system. Solar Energy 1999;65:171–80.
[29] Fukai J, Oishi A, Kodama Y, Kanou M, Miyatake O. Improvement of discharge characteristics of latent heat thermal storage unit by using carbon fibers. In: Proceedings of the 5th ASME/JSME Joint Thermal Engineering Conference; 1999.p. 7 (CD ROM, paper AJTE99-6338).
[30] Fukai J, Kanou M, Kodama Y, Miyatake O. Thermal conductivity enhancement of energy storage media using carbon fibers. Energy Conversion and Management 2000;41:1543–56.

[31] Cabeza LF, Mehling H, Hiebler S, Ziegler F. Heat transfer enhancement in water when used as pcm in thermal energy storage. Applied Thermal Engineering 2002;22:1141–51.
[32] Ettouney HM, Alatiqi I, Al-Sahali M, Al-Ali SA. Heat transfer enhancement by metal screens and metal spheres in phase change energy storage systems. Renewable Energy 2004;29:841–60.
[33] Stritih U. An experimental study of enhanced heat transfer in rectangular PCM thermal storage. International Journal of Heat and Mass Transfer 2004;47:2841–7.
[34] Koizumi H. Time and spatial heat transfer performance around an isothermally heated sphere placed in a uniform, downwardly directed flow (in relation to the enhancement of latent heat storage rate in a spherical capsule). Applied Thermal Engineering 2004;24:2583–600.
[35] Mesalhy O, Lafdi K, Elgafy A, Bowman K. Numerical study for enhancing the thermal conductivity of phase change material (PCM) storage using high thermal conductivity porous matrix. Energy Conversion and Management 2005;46:847–67.
[36] Khodadadi JM, Zhang Y. Effects of buoyancy-driven convection on melting within spherical containers. International Journal of Heat and Mass Transfer 2001;44:1605–18.
[37] Ettouney HI, Alatiqi M, Al-Sahali M, Al-Hajirie K. Heat transfer enhancement in energy storage in spherical capsules filled with paraffin wax and metal beads. Energy Conversion and Management 2006;47:211–28.
[38] Nayak KC, Saha SK, Srinivasan K, Dutta P. A numerical model for heat sinks with phase change materials and thermal conductivity enhancers. International Journal of Heat and Mass Transfer 2006;49:1833–44.
[39] Nakaso K, Teshima H, Yoshimura A, Nogami S, Hamada Y, Fukai J. Extension of heat transfer area using carbon fiber cloths in latent heat thermal energy storage tanks. Chemical Engineering and Processing 2008;47:879–85.
[40] Agyenim F, Eames P, Smyth M. A comparison of heat transfer enhancement in a medium temperature thermal energy storage heat exchanger using fins. Solar Energy 2009;83:1509–20.